Role of the Diphosphine Chelate in Emissive, Charge-Neutral Iridium(III) Complexes

Jia-Ling Liao,[a] Leon R. Devereux,[b] Mark A. Fox,[b,*] Chun-Chieh Yang,[c] Yu-Cheng Chiang,[c] Chih-Hao Chang,[c,*] Gene-Hsiang Lee[d] and Yun Chi[a,*]

[a] Department of Chemistry, National Tsing Hua University, Hsinchu 30013, Taiwan; E-mail: ychi@mx.nthu.edu.tw; ORCID id: orcid.org/0000-0002-8441-3974

[b] Department of Chemistry, Durham University, South Rd, Durham, DH1 3LE, UK; E-mail: m.a.fox@durham.uk; ORCID id: orcid.org/0000-0002-0075-2769

[c] Department of Photonics Engineering, Yuan Ze University, Chung-Li 32003, Taiwan; E-mail: chc@saturn.yzu.edu.tw; ORCID id: orcid.org/0000-0002-5586-9526

[d] Instrumentation Center, National Taiwan University, Taipei 10617, Taiwan.

Abstract

A class of neutral tris-bidentate Ir(III) metal complexes incorporating a diphosphine as a chelate is prepared and characterized here for the first time. Treatment of [Ir(dppBz)(tht)Cl_3] (**1**, dppBz = 1,2-bis(diphenylphosphino)benzene, tht = tetrahydrothiophene) with fppzH (3-trifluoromethyl-5-(2-pyridyl)-1*H*-pyrazole) afforded the dichloride complexes, *trans*-(Cl,Cl)[Ir(dppBz)(fppz)Cl_2] (**2**) and *cis*-(Cl,Cl)[Ir(dppBz)(fppz)Cl_2] (**3**). The reaction of **3** with the dianionic chelate precursor, 5,5'-di(trifluoromethyl)-3,3'-bipyrazole (bipzH_2) or 5,5'-(1-methylethylidene)-bis(3-trifluoromethyl-1H-pyrazole) (mepzH_2), in DMF gave the tris-bidentate complex [Ir(dppBz)(fppz)(bipz)] (**4**) or [Ir(dppBz)(fppz)(mepz)] (**5**), respectively. In contrast, a hydride complex [Ir(dppBz)(fppz)(bipzH)H] (**6**) was isolated instead of **4** in protic solvent, namely: diethylene glycol monomethyl ether (DGME). All complexes **2** - **6** are luminescent in powder forms and thin films where the dichlorides (**2**, **3**) emit with maxima at 590-627 nm (orange) and quantum yields (Q.Y.s) up to 90% whereas the tris-bidentate (**4**, **5**) and hydride (**6**) complexes emit at 455-458 nm (blue) with Q.Y.s up to 70%. Hybrid (time-dependent) DFT calculations showed considerable metal-to-

ligand charge transfer contribution to the orange-emitting **2** and **3** but substantial ligand-centered $^3\pi\pi^*$ transition character in the blue-emitting **4** - **6**. The dppBz does not participate to these radiative transitions in **4** - **6**, but it provides the rigidity and steric bulk needed to promote the luminescence by suppressing the self-quenching in the solid state. Fabrication of an OLED with dopant **5** gave a deep blue CIE chromaticity of (0.16, 0.15). Superior blue emitters, which are vital in OLED applications, may be found in other neutral Ir(III) complexes containing phosphine chelates.

Introduction

Iridium(III) metal complexes showing strong emissions in both fluid and solid states have been subjected to extensive investigations during the past two decades. Technological applications are demonstrated by the successful fabrication of optoelectronic devices such as light emitting electrochemical cells (LECs)[1] and organic light emitting diodes (OLEDs).[2] Chelates are one key component in assembling luminescent metal complexes, hence selecting chelates with distinctive electronic and steric properties are highly valuable in the design strategy.[3]

Neutral tris-bidentate Ir(III) complexes are generally luminescent, have high thermal stability and are relatively volatile which make them well-suited for fabrication of OLED devices through thermal evaporation. Therefore, thousands of charge-neutral tris-bidentate Ir(III) complexes with three monoanionic chelates - which can be identical (homoleptic) or different (heteroleptic) and can be *mer*- and *fac*-coordination isomers - have been synthesized due to their potential as suitable dopants in OLEDs.[4] Chart 1 shows the most popular chelates used in literature.[5] For example, 2-phenylpyridine (ppyH) and N-phenylpyrazole (ppzH) reacts with $IrCl_3$ via cyclometalation to give the ubiquitous green-emitting $Ir(ppy)_3$ at RT and blue-emitting $Ir(ppz)_3$ at 77 K, where ppy and ppz are monoanionic *C*,*N*-chelate.[6]

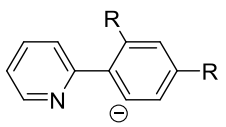

R = H; 2-phenylpyridyl, ppy
R = F; F2ppy

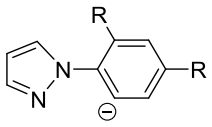

R = H; 1-phenylpyrazolyl, ppz
R = F; F2ppz

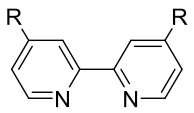

R = H; bipyridyl, bpy
R = Bu^t; dtbbpy

Chart 1: Common anionic and neutral chelates in preparation of tris-bidentate Ir(III) complexes.

Cationic tris-bidentate Ir(III) complexes can also be luminescent but they are less volatile thus are generally less desirable for OLED applications.[1d] These cationic complexes have been made using many charge-neutral chelates such as 2,2'-bipyridine (bpy). This latter ligand forms relatively strong metal-chelate bonding with lower-lying π*-orbital, which are capable to facilitate effective metal-to-ligand charge transfer (MLCT) transition, an essential component in inducing strong luminescence of transition metal complexes.[1, 7]

For charge-neutral tris-bidentate Ir(III) complexes containing both neutral and anionic chelates, the third chelate would inevitably be dianionic. The first charge-neutral tris-bidentate Ir(III) complexes with dianionic chelates were synthesized recently as [Ir(dtbbpy)(ppy)(bipz)] **A** and [Ir(dtbbpy)(ppy)(mepz)] **B** in high yields (Chart 2).[8] The dianionic chelates, bipz and mepz, were obtained from 5,5'-di(trifluoromethyl)-3,3'-bi-pyrazole ($bipzH_2$) and 5,5'-(1-methylethylidene)-bis(3-trifluoromethyl-1H-pyrazole) ($mepzH_2$) respectively.[9] These charge-neutral tris-bidentate Ir(III) complexes **A** and **B** were shown to have quantum yields up to 88% in films, and OLEDs fabricated with these complexes as dopants gave yellow-green luminescence with CIE chromaticities of (x = 0.38-0.41, y = 0.58-0.56).

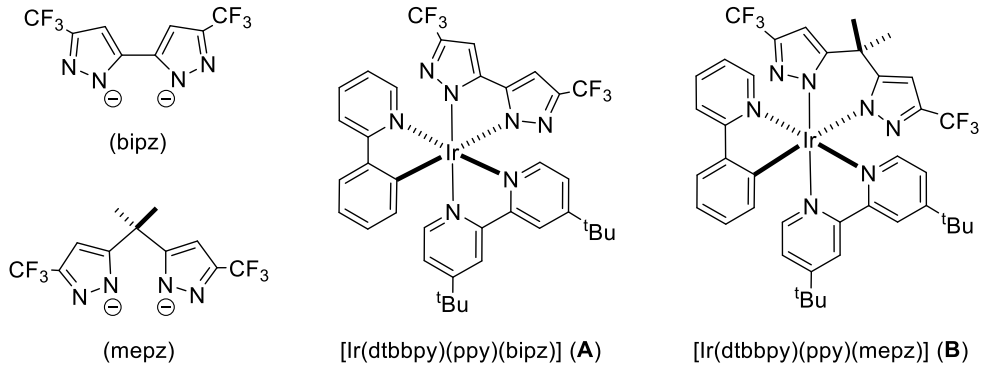

Chart 2: Bipz and mepz chelates and the tris-bidentate Ir(III) complexes with neutral, anionic and dianionic chelates.

We were interested in creating blue emitters based on the new tris-bidentate Ir(III) design consisting of neutral, anionic and dianionic chelates to be used in efficient blue OLEDs. All the neutral, anionic and dianionic chelates would therefore require larger energy gaps for high energy (blue) phosphorescence. Here, both the neutral dtbbpy and anionic ppy chelates of the reported complexes **A** and **B** are replaced by 1,2-bis(diphenylphosphino)benzene[10] (dppBz) and 3-trifluoromethyl-5-(2-pyridyl)-1*H*-pyrazolate (fppz)[6c, 7, 11] chelates respectively. While there are many known cationic tris-bidentate Ir(III) complexes with diphosphine chelates,[12] surprisingly no charge-neutral tris-bidentate Ir(III) complex containing a diphosphine chelate had been reported before this study. Furthermore, the reaction pathways en route to the final emissive products are established, opening new horizons for the strategic tuning of molecular organization and design of luminescent materials.

Results and Discussion

Syntheses and characterizations. The complex $[Ir(tht)_3Cl_3]$, tht = tetrahydrothiophene, was first reacted with an equal amount of 1,2-bis(diphenylphosphino)benzene (dppBz) to afford $[Ir(tht)(dppBz)Cl_3]$ (**1**). Its structure is akin to that of the di-substitution product $[Ir(tht)(PPh_3)_2Cl_3]$ obtained from treatment of $[Ir(tht)_3Cl_3]$ with two equivalents of PPh_3.[13] The dppBz complex **1** possesses three chloride ligands arranged in the meridional geometry. This structure

is verified by NMR spectroscopies where peaks corresponding to a 1:1 ligand ratio of tht: dppBz are shown in the ^{1}H NMR spectrum and two set of doublets at δ 15.43 and 9.85 (J_{PP} = 2.9 Hz) for chemically distinct phosphorus atoms are present in the ^{31}P NMR spectrum.

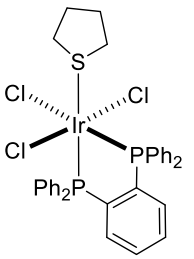

[Ir(tht)(dppBz)Cl_3] (**1**)

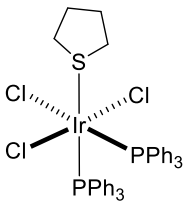

[Ir(tht)(PPh_3)$_2Cl_3$]

Heating complex **1** with fppzH in refluxing DMF for 6 h afforded *trans*-(Cl,Cl) [Ir(dppBz)(fppz)Cl_2] (**2**) while changing the solvent to the high-boiling diethylene glycol monomethyl ether (DGME) afforded *cis*-(Cl,Cl) [Ir(dppBz)(fppz)Cl_2] (**3**) in comparable yields. Complexes **2** and **3** are the kinetic and thermodynamic products respectively as **2** can be converted to **3** by extensive heating in boiling DGME. The addition of excess NaCl in DGME was necessary to suppress decomposition induced by chloride dissociation in this thermal isomerization process. The formation of the kinetic product **2** reflects weaker metal-ligand bonds involving the tht ligand and the chloride opposite to the PPh_2 fragment in **1** compared to the *trans*-substituted chloride ligands.

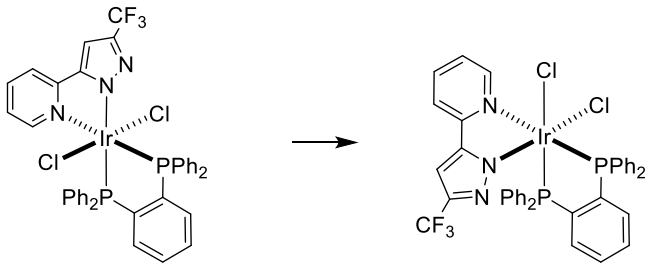

trans-[Ir(dppBz)(fppz)Cl_2] (**2**) *cis*-[Ir(dppBz)(fppz)Cl_2] (**3**)

The molecular structures of **2** and **3** are shown in Figures 2 and 3 respectively. The dppBz and fppz chelates of **2** take the square planar disposition while the dppBz and fppz chelates of **3** take the orthogonal orientation with the unique pyridyl fragment of fppz chelate located opposite to one of the PPh_2 fragment. The *trans*-Ph_2P-Ir-N(pz)

ligand arrangement in **2** with two stronger PPh_2 and N(pz) donor atoms located at the *trans*-disposition (cf. Ir-N(2) = 2.058(4) Å and Ir-P(1) = 2.3057(12) Å), is replaced by the *trans*-Ph_2P-Ir-Cl and *trans*-N(pz)-Ir-Cl arrangements in **3**, with corresponding P-Ir and N-Ir distances being substantially shorter (cf. Ir-N(2) = 2.021(3) Å and Ir-P(2) = 2.2544(8) Å). Thus, this change of ligand arrangement and coordination bond strength is the driving force for the thermally induced isomerization. Formation of **3** via the less stable intermediate **2** is conceptually similar to that of the meridional-to-facial isomerization of homoleptic Ir(III) cyclometalate complexes,[6a] as well as the thermally induced isomerization of heteroleptic Ir(III) metal complexes.[14] Concomitantly, the Ir-Cl distances increased from Ir-Cl(1) = 2.3548(11) Å and Ir-Cl(2) = 2.3661(12) Å in **2** to Ir-Cl(1) = 2.3648(8) Å and Ir-Cl(2) = 2.4240(8) Å in **3**. Since the chlorides are generally considered as weak field ligands, the variation in their distances is expected to impose only minor influence to the overall stabilities.

The Ir(III) complexes [Ir(dppBz)(fppz)(bipz)] (**4**) and [Ir(dppBz)(fppz)(mepz)] (**5**) were synthesized by heating **3** with the *in situ* prepared disodium salts of 5,5'-di(trifluoromethyl)-3,3'-bipyrazolate ($bipzNa_2$) and 5,5'-(1-methylethylidene)bis(3-trifluoromethyl-1H-pyrazolate) ($mepzNa_2$) in refluxing DMF, respectively. The ^1H and ^{19}F NMR spectra showed incorporation of the dianionic chelates bipz and mepz for **4** and **5**, respectively and their structures were also confirmed by single crystal X-ray structural analyses as depicted in Figures 3 and 4. Both dppBz and fppz chelates retain their initial disposition, while the incoming bipz and mepz chelates take up positions originally occupied by *cis*-substituted chlorides of **3**. Hence, the formation of **4** or **5** is best described as a simple substitution reaction. With respect to the metric parameters, the metal-ligand bonding imposed by the bipz and mepz chelates are stronger than the metal-chloride bonds in **3**. Therefore, the metal-ligand distances of *trans*-PPh_2 and *trans*-N(pz) donor atoms in **4** and **5** (Ir-P(1) = 2.2914(14) Å and Ir-N(2) = 2.047(5) Å for **4** and Ir-P(1) = 2.3007(10) Å and Ir-N(2) = 2.044(3) Å for **5** are longer than those in the dichloride complex **3** (Ir-P(2) = 2.2544(8) Å and Ir-N(2) = 2.021(3) Å).

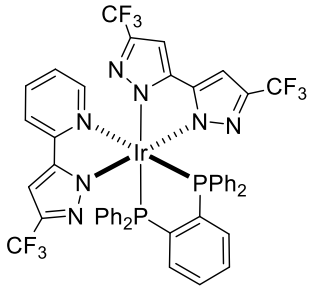

[Ir(dppBz)(fppz)(bipz)] (**4**)

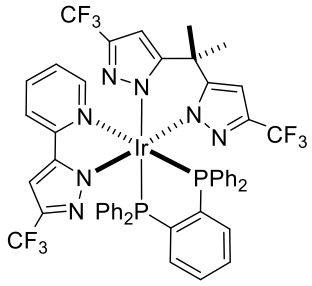

[Ir(dppBz)(fppz)(mepz)] (**5**)

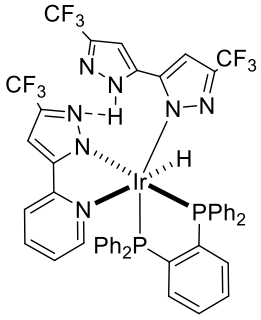

[Ir(dppBz)(fppz)(bipzH)H] (**6**)

In contrast to the simple ligand substitution for the formation of **4** in refluxing DMF as well as the formation of **5** from heating of **3** with mepzNa_2 in both DMF and DGME, heating of **3** with bipzNa_2 in diethylene glycol monomethyl ether (DGME) unexpectedly gave a distinctive Ir(III) metal-hydride complex [Ir(dppBz)(fppz)(bipzH)H] (**6**) in 47% yield. This complex showed two unique ^{1}H NMR signals at δ 14.85 and −18.69 (dd, J_{HP} = 23.6, 16.3 Hz) in CD_2Cl_2 which are assigned to the pyrazolic proton and metal hydride respectively based on their characteristic chemical shifts and J_{HP} coupling patterns. Formation of the metal hydride **6** is probably induced by the hydroxy group of DGME.[15] The structure of **6** was confirmed by single-crystal X-ray diffraction as shown in Figure 5, for which the core arrangement of **6** is clearly different from those observed for Ir(III) complexes **3**, **4** and **5**. As can be seen, the bipzH fragment, pyrazolate of fppz chelate and hydride formed a triangular arrangement. An intramolecular N-H···N interaction between the pyrazolic hydrogen of bipzH and a pyrazolyl nitrogen of the fppz ligand is present in **6** and with distances of N(6)-H(6) = 0.75(4) Å and N(3)···H(6) = 2.02(4) Å.

The DGME solvent provided a fast chloride-to-hydride substitution (due to its protic nature) followed by chelate isomerization during the addition of the monodentate bipzH ligand to afford the hydride complex **6** with the observed *cis*-H-Ir-N(pz) and *trans*-H-Ir-N(py) geometry. This hypothesis is supported by:

(i) the slower conversion from **3** to **6** in DGME (194 °C, 12 h) vs. the faster formation of **4** in lower boiling DMF solvent (153 °C, 12 h),

(ii) the failure in inducing the **4** to **6** transformation in refluxing DGME solution, even

in the presence of an hydride source $NaBH_4$, for which both reactions were conducted at 190 °C and over a period of 24 h, and

(iii) heating of **6** in DMF afforded **4** in 25 % yield thus confirming the facile elimination of adjacent hydride and proton in DMF along with chelate rearrangement.

A simplified reaction scheme is depicted in Scheme 1 to show the stepwise conversion from dppBz starting material **1**, to dppBz intermediates **2** and **3**, and the sequence and experimental condition that afforded the final mepz and bipz products **4**, **5** and **6**.

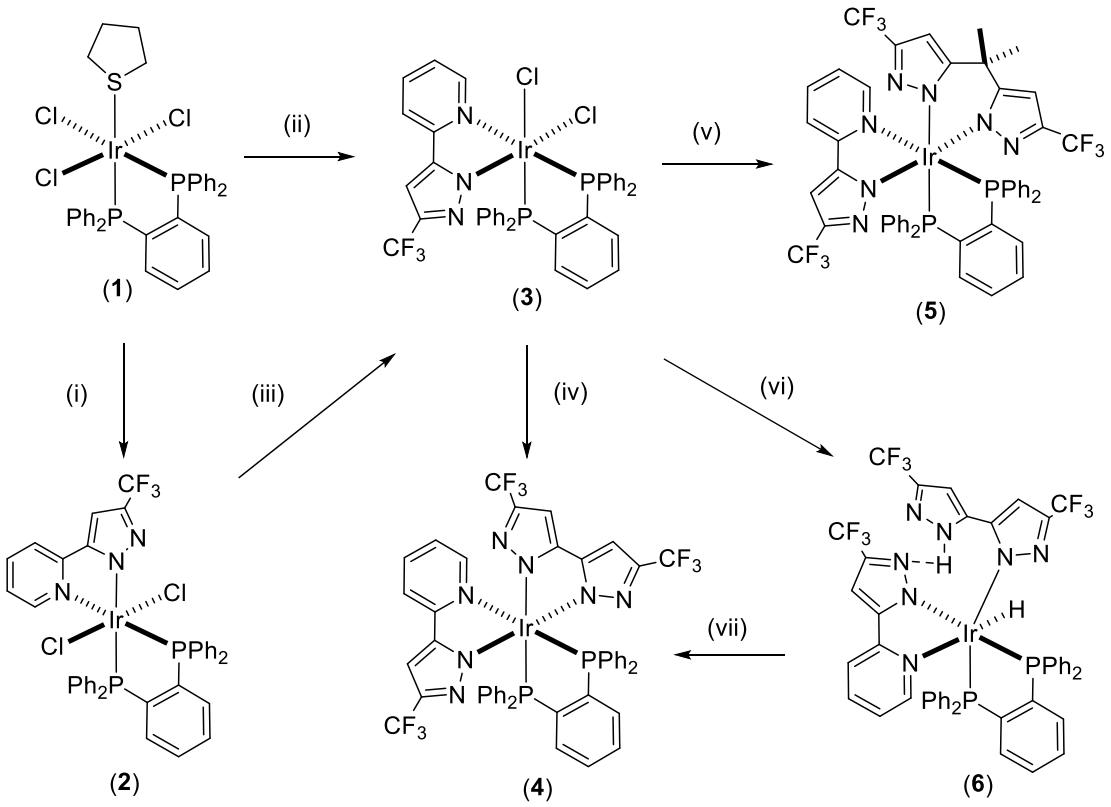

Scheme 1. Transformation of the studied Ir(III) complexes **1** - **6**; experimental conditions: (i) fppzH, DMF, 6 h, 153°C. (ii) fppzH, DGME, 6 h, 194°C. (iii) DGME, NaCl, 12h, 194°C. (iv) $bipzNa_2$, DMF, 12 h, 153°C. (v) $mepzNa_2$, DMF, 12 h, 153°C. (vi) $bipzNa_2$, DGME, 12 h, 190°C. (vii) K_2CO_3, DMF, 24 h, 153°C.

Photophysical Properties. The UV-Vis spectra of Ir(III) complexes **2** - **6** recorded in CH_2Cl_2 are depicted in Figure 6 and the numerical data summarized in Table 1. On first impression, all complexes show similar absorption profiles, and all Ir(III)

complexes exhibit extremely weak emission in degassed solutions at RT and, hence, only emission spectra of the powder forms and in PMMA matrix were reported (Table 1). In general, the higher emission quantum yields (Q.Y., Φ) against those recorded in fluid states are caused by the rigid environments which are expected to restrict the lengthening of metal-ligand bonding upon excitation and, in turn, to destabilize the MC *dd* excited states.[16] No change in the emission profiles was observed between the powder spectra and those measured in PMMA matrix in all cases which imply that no notable intermolecular stacking interactions are present within this class of Ir(III) metal complexes.

Broad emission bands at 627 nm and 590 nm in powder (Figure 6) and at 630 nm and 592 nm in PMMA were observed for the *trans*-**2** and *cis*-**3** dichlorides respectively. The broad profiles are consistent with a dominant MLCT emission from the excited states. Upon replacement of the chlorides with anionic N-donors such as bipz, mepz and bipzH, substantial blue-shifts in emissions were found for Ir(III) complexes **4**, **5** and **6**. All these Ir(III) complexes revealed identical emission profiles but with variable Q.Y.s (Φ) and radiative rate constants (k_r) in the solid state at RT, cf. 1 x 10^4 s^{-1} for **4**, 1.3 x 10^4 s^{-1} for **5** and 0.92 x 10^4 s^{-1} for **6**, calculated using the equation $k_r = \Phi/\tau_{obs}$. The observed vibronic emission profiles imply greater ligand-centered ππ* contribution in the excited states and smaller radiative rate constants. These behaviors suggest less heavy-metal atom induced spin-orbital couplings and thus less MLCT contributions to the excited states. The higher radiative rate constant of **5** compared to **4** and **6** also suggests that complex **5** is the most suitable blue phosphor among the three for OLED fabrications. Furthermore, these dppBz complexes seem to have superior emission efficiencies vs. the bpy-based Ir(III) complexes **A** and **B**, for which the stronger ligand field strength of dppBz chelate would destabilize the metal-centered dd excited state and giving reduced thermal quenching.

Electrochemical Studies. Cyclic voltammetry measurements were carried out on Ir(III) complexes **2** - **6** (Figure S1) with their oxidation and reduction potentials listed in Table 1. The oxidation potentials for all complexes are virtually identical at 1.2 V except

for complex **4** which is oxidized more easily by ca 0.15 V. This suggests that the HOMO for **4** is higher in energy than the other complexes which may be attributed to the more electron-donating dianionic bipz chelate present. The reduction potentials at ca -2.6 V are similar in **4** - **6**, implying that their LUMOs are similar and presumably are on the fppz chelate. Reductions of the dichlorides **2** and **3** are considerably more facile at ca -2.2 V with differences of ca 0.4 V compared to complexes **4** - **6**. Based on the assumption that the negative potentials mirror the LUMO energies, the LUMOs in **2** and **3** presumably involve the chlorides.

Computations. Calculated energies of the *trans*-**2** and *cis*-**3** reveal that the latter is more stable by 5.1 kcal mol^{-1} confirming that the structural isomer **3** is more thermodynamically stable than **2** as found experimentally. The alternative isomers of **4** and **6** as complexes **7** and **8** respectively were also computed to estimate the relative energies and show whether **7** and **8** could be isolated experimentally. Geometry of **4** is more stable than geometry of **7** by 2.3 kcal mol^{-1} whereas **6** is more stable than **8** by 9.7 kcal mol^{-1}. It is likely that chelate rearrangements are facile in these complexes favoring the more thermodynamically stable isomers **4** and **6** observed experimentally.

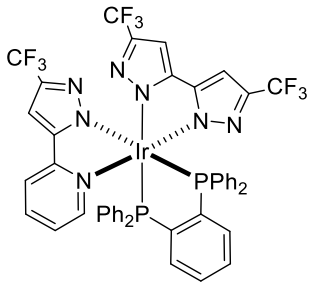

[Ir(dppBz)(fppz)(bipz)] (**7**)

alternate fppz orientation

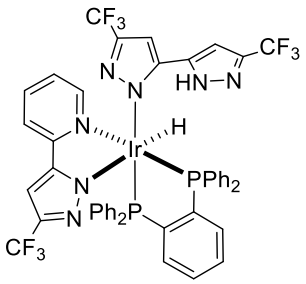

[Ir(dppBz)(fppz)(bipzH)H] (**8**)

alternate fppz orientation

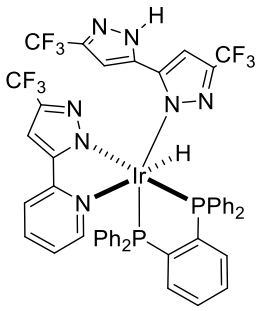

[Ir(dppBz)(fppz)(bipzH)H] (**9**)

no N-H···N interaction

The large difference in energy between **6** and **8** may partly be attributed to the favorable N-H···N intramolecular interaction observed in the X-ray crystal structure. This favorable interaction is computed at 5.4 kcal mol^{-1} by comparing the optimized

geometry of **6** with that of **9** where the pyrazolyl group is twisted so that there is no N-H···N intramolecular interaction. In fact, **9** is more energetically stable than **8** by 4.2 kcal mol^{-1} thus the *trans* orientation between the hydride and the pyridyl group is strongly favored.

Both HOMOs and LUMOs in the dichlorides (**2** and **3**) have substantial metal contributions (Figure 7 and Table S1). While the HOMOs are similar in both dichloride isomers, the LUMOs in these dichloride complexes are very different with the LUMO of the *cis* isomer **3** involving fppz/dppBz ligands and iridium, whereas the LUMO of **2** has mixed metal-chloride character. By contrast, the frontier orbitals for the blue emitters (**4** - **6**) contain little metal character (Figure 8 and Table S2). The HOMOs of the blue emitters are located at the bipz/mepz/bipzH ligand, whereas all their LUMOs are at the fppz ligand. The agreement between computed HOMO energies and observed oxidation potentials of **2** - **6** from cyclic voltammetry is excellent (Table S3).

The low energy bands in the observed absorption spectra are discussed here for comparison with computed TD-DFT data. In the dichloride complexes, *trans* **2** showed an observed lowest energy absorption edge at 380 nm whereas *cis* **3** has the edge at 410 nm (Figure S2). TD-DFT results predict 501 nm for **2** and 416 nm for **3** corresponding to their $S_0 \rightarrow T_1$ (HOMO $\rightarrow$ LUMO) absorption transitions which are mixed metal-chloride to mixed metal-chloride (^{3}MX $\rightarrow$ MX) for **2** and mixed metal-chloride to metal-fppz ligand (^{3}MX $\rightarrow$ ML) for **3** (Figure 7). The absence of low energy absorptions observed for **2** suggest that the low energy triplet transitions in *trans* **2** are much weaker than in *cis* **3** due to the different LUMOs involved in the transitions.

The observed lowest energy absorption edge wavelengths for **4** and **5** at ca 380 nm are similar to **2** and correspond well with TD-DFT $S_0 \rightarrow T_1$ wavelength predictions at 406 nm and 410 nm. However, the nature of the $S_0 \rightarrow T_1$ transitions in these blue emitters is not dominated by HOMO to LUMO transitions. The HOMO-1s which are

located on the fppz ligands contribute significantly to these transitions instead of the bipz/mepz centered HOMOs (Figure 8). The observed short edge wavelength at 355 nm for **6** is intriguing and suggests that the bands corresponding to triplet MLCT transitions in **6** must be very weak or absent. The computed TD-DFT $S_0 \rightarrow T_1$ wavelength of 392 nm for **6** is relatively short compared to the wavelengths for **4** and **5**. The lowest energy absorption maxima for all complexes in Table 2 were determined using Gaussian deconvolution analyses (Figures S3 – S7) and they correspond well with low energy $S_0 \rightarrow S_n$ transitions of relatively high oscillator strengths from TD-DFT computations where they are considered as ^{1}MLCT (Table 2). The more intense bands observed at 260 - 310 nm arise from ligand-centered ππ* transitions.

The T_1 excited state geometries are assumed here to change little compared to the S_0 ground state geometries thus the nature of emissive transitions are presumed to mirror those on absorptions here. For this assumption to be valid, the observed Stokes shifts should be low in energies. The observed Stokes shift energies for the dichloride complexes are large at ca 11000 cm^{-1} for **3** and 13500 cm^{-1} for **2** (Table 2). Thus, the T_1 excited state geometries for these dichloride complexes are likely to be substantially different to their S_0 ground state geometries. The smaller Stokes shift energies of ca 5100 to 7300 cm^{-1} observed for the blue emitters indicate that their T_1 excited state geometries are similar to their S_0 ground state geometries. There is therefore an excellent agreement between observed and calculated TD-DFT $S_0 \leftarrow T_1$ emission wavelengths for the blue emitters.

The broad emission profiles observed for the dichloride complexes arise from the substantial MLCT contributions in the excited states whereas the emissions with vibronic structure for the blue emitters are due to largely ligand-centered ππ* contributions in the excited states according to computations. The faster observed lifetimes for the dichlorides (2.8 - 3.8 μs) compared to the blue emitters (51 - 75 μs)

explained by large MLCT contributions in the dichlorides is supported by TD-DFT data here.

OLED Device Fabrications. Ir(III) phosphor **5** with a high quantum yield of 70% in powder form (Table 1) was selected in the fabrication of true-blue phosphorescent organic light-emitting diodes (PhOLEDs). In general, deep-blue or true-blue phosphors should be combined with host material of triplet gap greater than 2.9 eV to achieve better exothermic energy transfer.[17] Furthermore, the employment of dual host materials with opposite carrier transport capabilities increases carrier recombination and widens the exciton formation zone in the emitting layers (EMLs) of OLEDs.[18] Therefore, in this study, both single-EML and double-EML structures were attempted. Based on our previous studies, two wide-gap hosts, 9-(4-tert-butylphenyl)-3,6-bis(triphenylsilyl)-9H-carbazole (CzSi) and bis(2-(diphenylphosphino)phenyl)ether oxide (DPEPO), were chosen as the principal emitting layer (EML1) and the accessory emitting layer (EML2) respectively.[19] The EML of devices B1 and B2 consists of (i) CzSi doped with 6 wt.% **5** (28 nm) and (ii) CzSi doped with 6 wt.% **5** (25 nm)/DPEPO doped with 6 wt.% **5** (3 nm). A thin layer of DPEPO was deposited at the interface between the EML and the electron transport layer (ETL) for better exciton confinement. On the other hand, di-[4-(N,N-ditolyl-amino)-phenyl]cyclohexane (TAPC) and 4,4',4"-tris(carbazol-9-yl)-triphenylamine (TCTA) were combined to form the stepped hole transport layers in facilitating efficient carrier injection from the ITO anode to the EML. In addition, 1,3,5-tri[(3-pyridyl)phen-3-yl]benzene) (TmPyPB) with a large triplet gap was used as the ETL.[20] Consequently, the resulting PhOLEDs possess the architecture: ITO (120 nm)/TAPC (30 nm)/TCTA (10 nm)/EML (28 nm)/DPEPO (2 nm)/TmPyPB (50 nm)/LiF (0.8 nm)/Al (150 nm), where LiF and Al served as the electron injection layer and cathode, respectively. Figure 9 presents both the molecular structures of the employed materials and the schematic OLED diagrams.

The electroluminescence (EL) characteristics and associated numerical data of the tested devices are shown in Figure 10 and Table 3. As shown in Figure 10(a), the EL

spectra of devices B1 and B2 exhibited solely the emission of **5**, confirming the effective exothermic energy transfer from host to dopant. Both devices B1 and B2 showed deep-blue emissions with CIE coordinates of (0.16, 0.16) and (0.16, 0.15), respectively. These coordinates are significantly blue-shifted compared to OLEDs made from the well-known heteroleptic iridium blue emitter FIrpic with coordinates typically at (0.17, 0.34).

Figure 10(b) exhibited the *J-V-L* curves of both tested devices, from which the slightly higher current density observed in device B2 indicates better electron transport. As shown in Figures 10(c) and (d), the maximum EL efficiencies of device B1 were recorded to be 6.5 %, 7.6 cd/A, and 6.1 lm/W, while at a practical brightness of 100 cd/m^2, the efficiencies dropped to around 2.3 %, 2.7 cd/A, and 1.1 lm/W, respectively. These characteristics are lower than those of device B2 with peak efficiencies of 9.6 %, 11.0 cd/A, and 9.6 lm/W, and the forward efficiencies of 3.8 %, 4.4 cd/A, and 2.2 lm/W at 100 cd/m^2. Clearly, a double EML structure of B2 has successfully boosted the efficiencies compared to a single EML structure of device B1.

These deep-blue OLEDs give us an opportunity to fabricate a white-emitting OLED (WOLED) with decent color rendering index (CRI) and correlated color temperature (CCT). In general, the CRI and CCT should exceed 80 and within 4000–6500 K respectively for domestic lighting applications.[21] Consequently, the bis-tridentate Ir(III) complex **10** with deep-red CIE coordinate (0.63, 0.37) and high quantum yield (Φ = 0.63),[22] for which its structural drawing is depicted in Figure 9(a), and commercially available [Ir(ppy)$_2$(acac)] were selected as the red- and green-emitting phosphors.[23] These emitters are next sandwiched between the dual EML (i.e. EML1 and EML2) of B2 to achieve stabilized white emission.[24] Therefore, the excitons are expected to occur at both EML1 and EML2, together with efficient energy transfer to the red and green dopants. The schematic architecture of this WOLED, ITO (120 nm)/TAPC (30 nm)/TCTA (10 nm)/CzSi doped with 6 wt.% **5** (23 nm)/CzSi doped with 0.5 wt.% [Ir(ppy)$_2$(acac)] (1 nm)/CzSi doped with 0.8 wt.% **10** (1 nm)/DPEPO doped with 6 wt.%

5 (3 nm)/DPEPO (2 nm)/TmPyPB (50 nm)/LiF (0.8 nm)/Al (150 nm), is depicted in Figure 9.

Figure 10(a) shows the EL spectra of WOLED (i.e. device W) at luminance of 300 and 500 cd/m^2, for which the emission are clearly derived from all RGB emitters, and showed the corresponding CRI and CCT of 90.7 and 5943K at 300 cd/m^2. The slightly superior device characteristics of W vs those of B2, shown in Figures 10(b-d), are probably due to the cascade energy transport and higher emission efficiencies of red and green dopants. A maximum external quantum efficiency of 13.0 %, luminance efficiency of 25.7 cd/A, and power efficiency of 22.4 lm/W were recorded for this WOLED and values of 7.0 %, 14.0 cd/A, and 7.2 lm/W respectively were obtained at a practical brightness of 100 cd/m^2.

Conclusions

In summary, our investigation demonstrated the successful preparation of two charge-neutral tris-bidentate Ir(III) complexes bearing 1,2-bis(diphenylphosphino)-benzene (dppBz) for the first time. The anionic pyridyl pyrazolate (fppz) and the dianionic 5,5'-di(trifluoromethyl)-3,3'-bipyrazolate (bipz) or 5,5'-di(trifluoromethyl)-3,3'-bipyrazolate (mepz) complete the remaining ligand coordination sites of Ir(III) complexes **4** and **5**. The Ir(III) complex **6** with an hydride and a monodentate pyrazole-pyrazolate ligand (i.e. bipzH) was obtained upon switching to DGME solvent. The dehydrogenation conversion of **6** to **4** is achieved by heating **6** in non-protic DMF, demonstrating the solvent-dependent synthetic protocol of this class of Ir(III) complexes.

Computations on the tris-bidentate Ir(III) complexes **4** – **6** revealed very good agreement with those observed using X-ray crystallography, cyclic voltammetry and photophysical data. The Ir(III) complexes **4** – **6** showed deep-blue emissions due to the larger energy gap and steric rigidity of dppBz vs. the neutral dtbbpy chelate in closely related yellow-green Ir(III) emitters **A** and **B**. The dianionic chelates, bipz and mepz, and the anionic chelate fppz unfortunately do not promote the MLCT needed for fast

phosphorescence. A more suitable anionic or dianionic chelate is needed in the Ir(III) diphosphine design to exploit the potential of Ir(III) diphosphine complexes in serving as the efficient blue emitters.

An OLED with a double EML configuration and dopant **5** (device B2) gave deep-blue CIE chromaticity of (0.16, 0.15) and a maximum external quantum efficiency (luminance efficiency and power efficiency) of 9.6 % (11.0 cd/A and 9.6 lm/W). In addition, the blue emission of **5** facilitated the fabrication of a white-emitting OLED by combining with a red-emitting Ir(III) phosphor **10** and a green-emitting [$Ir(ppy)_2(acac)$]. This three-component WOLED presented stable and broadened emission with CIE of (0.32, 0.34), high CRI and CCT of 90.7 and 5943 K, and peak performances of 13.0%, 25.7 cd/A, and 22.4 lm/W, respectively. Overall, these results suggest high potential of Ir(III) diphosphine design in fabrication of efficient blue and white-emitting OLEDs.

Experimental Section

General Information and Materials. All reactions were conducted under N_2 atmosphere using anhydrous solvents or solvents treated with an appropriate drying reagent. Commercially available reagents were used without purification unless otherwise stated. 5,5'-di(trifluoromethyl)-3,3'-bipyrazole ($bipzH_2$)[25] and 5,5'-(1-methylethylidene)bis(3-trifluoromethyl-1H-pyrazole) ($mepzH_2$)[26] were prepared according to literature procedures. Deprotonation of biazole chelates (e.g. $bipzH_2$ and $mepzH_2$) was executed using NaH in anhydrous THF at 0 °C. After filtering of the unreacted NaH, evaporation of THF afforded the crude biazolates (e.g. $bipzNa_2$ and $mepzNa_2$) that were used without further purification. Mass spectra were obtained on a JEOL SX-102A instrument operating in electron impact (EI) or fast atom bombardment (FAB) mode. ^1H, ^{19}F, and ^{31}P NMR spectra were obtained using the Varian INOVA-500 instrument. Elemental analyses were performed using the Heraeus CHN-O rapid elementary analyzer. Cyclic voltammetry measurements were carried out on a CHI621A Electrochemical Analyzer. Steady-state absorption and emission spectra were recorded with a Hitachi (U-3900) spectrophotometer and an Edinburgh (FS920)

fluorimeter, respectively. Detailed electrochemical and photophysical procedures are in the electronic supporting information.

Preparation of [Ir(dppBz)(tht)Cl_3] (1). A mixture of 1,2-bis(diphenylphosphino)-benzene (dppBz, 793 mg, 1.78 mmol) and [Ir(tht)$_3Cl_3$] (1.0 g, 1.78 mmol) in decalin (70 mL) was refluxed for 6 hr. After cooled to RT, the yellow precipitate was filtered and washed with diethyl ether. The crude product [Ir(dppBz)(tht)Cl_3] (1.33 g, 1.60 mmol, 90%) was used for the next reaction without further purification.

Spectroscopic data for 1: ^{1}H NMR (500 MHz, CD_2Cl_2, 294 K): δ 7.72 70 ~ 7.58 (m, 8H), 7.57~ 7.53 (m, 4H), 7.42 ~ 7.40 (m, 4H), 7.34 ~ 7.30 (m, 8H), 3.68 (br, 2H), 2.49 (br, 2H), 2.15 (br, 2H), 1.91 (br, 2H). ^{31}P NMR (202 MHz, CD_2Cl_2, 294 K): δ 15.43 (d, J_{PP} = 2.9 Hz, 1P), 9.85 (d, J_{PP} = 2.9 Hz, 1P).

Preparation of *trans*-(Cl,Cl) [Ir(dppBz)(fppz)Cl_2] (2). A mixture of [Ir(dppBz)(tht)Cl_3] (1.2 g, 1.44 mmol) and fppzH (323 mg, 1.52 mmol) in anhydrous DMF (60 mL) was refluxed for 6 hr. After cooled to RT, the solution was partially concentrated and the addition of 20 mL of diethyl ether gave a pale yellow precipitate that was filtered and washed with diethyl ether. The crude product was subjected to silica gel column chromatography using a 2:3 mixture of ethyl acetate and hexane as the eluent. The yellow crystals of **2** were obtained from a mixture of CH_2Cl_2 and hexane (940 mg, 1.01 mmol, 70%).

Data for 2: MS (FAB, ^{192}Ir): *m/z* 922 [M^+]. ^{1}H NMR (500 MHz, CD_2Cl_2, 294 K): δ 8.62 (t, *J* = 4.4 Hz, 1H), 7.84 (t, *J* = 7.6 Hz, 1H), 7.79 ~ 7.75 (m, 5H), 7.70 ~ 7.61 (m, 7H), 7.49 (t, *J* = 7.2 Hz, 3H), 7.38 (t, *J* = 6.6 Hz, 6H), 7.29 (t, *J* = 7.6 Hz, 4H), 6.94 (t, *J* = 6.6 Hz, 1H), 6.90 (s, 1H). ^{19}F NMR (470 MHz, CD_2Cl_2, 294 K): δ -61.20 (s, 3F). ^{31}P NMR (202 MHz, CD_2Cl_2, 294 K): δ 6.59 (s, 1P), 5.88 (s, 1P). Anal. Calcd. for $C_{39}H_{29}Cl_2F_3IrN_3P_2$: C, 50.82; H, 3.17; N, 4.56. Found: C, 51.26; H, 3.60; N, 5.00.

Selected crystal data of 2: $C_{43}H_{39}Cl_2F_3IrN_3OP_2$; M = 995.81; monoclinic; space group = C2/c; *a* = 32.6514(4) Å, *b* = 14.4369(2) Å, *c* = 19.9819(3) Å, β = 119.2849(6)°, *V* = 8215.4(2) Å^3; *Z* = 8; ρ_{calcd} = 1.610 Mg·m^{-3}; *F*(000) = 3952; crystal size = 0.28 × 0.18 ×

0.13 mm^3; λ(Mo-Kα) = 0.71073 Å; T = 150(2) K; μ = 3.510 mm^{-1}; 24869 reflections collected, 9386 independent reflections (R_{int} = 0.0493), GOF = 0.954, final $R_1[I > 2\sigma(I)]$ = 0.0364 and wR_2(all data) = 0.0997.

Preparation of *cis*-(Cl,Cl) [Ir(dppBz)(fppz)Cl_2] (3). Method 1: A mixture of [Ir(dppBz)(tht)Cl_3] (110 mg, 0.13 mmol) and fppzH (31 mg, 0.14 mmol) in DGME (10 mL) was refluxed for 6 hr. After removed of solvent, the residue was washed with diethyl ether. The crude product was subjected to silica gel column chromatography using a 2:3 mixture of ethyl acetate and hexane as the eluent. The yellow crystals of **3** were obtained from a mixture of CH_2Cl_2 and hexane (86 mg, 0.09 mmol, 71%).

Method 2: A solution of **2** (540 mg, 0.59 mmol) and NaCl (340 mg, 5.9 mmol) in DGME (30 mL) was refluxed for 12 hr. The mixture was next concentrated *in vacuo*, and the residue was subjected to silica gel column chromatography eluting with a 1:1 mixture of CH_2Cl_2 and hexane. The yellow crystals of **3** were obtained from a mixture of CH_2Cl_2 and hexane (350 mg, 0.38 mmol, 60%).

Data for 3: MS (FAB, ^{192}Ir): *m*/*z* 922 [M^+]. ^{1}H NMR (500 MHz, CD_2Cl_2, 294 K): δ 9.29 (t, *J* = 4.3 Hz, 1H), 7.93 ~ 7.81 (m, 4H), 7.74 ~ 7.70 (m, 3H), 7.62 (t, *J* = 7.8 Hz, 1H), 7.55 (t, *J* = 7.9 Hz, 1H), 7.50 ~ 7.33 (m, 10H), 7.29 ~ 7.25 (m, 3H), 7.18 (t, *J* = 7.3 Hz, 1H), 6.87 (t, *J* = 7.9 Hz, 2H), 6.58 ~ 6.54 (m, 2H), 6.39 (s, 1H). ^{19}F NMR (470 MHz, CD_2Cl_2, 294 K): δ -61.79 (s, 3F). ^{31}P NMR (202 MHz, CD_2Cl_2, 294 K): δ 15.44 (d, J_{PP} = 4.0 Hz, 1P), 14.41 (d, J_{PP} = 4.0 Hz, 1P). Anal. Calcd. for $C_{39}H_{29}Cl_2F_3IrN_3P_2$: C, 50.82; H, 3.17; N, 4.56. Found: C, 50.55; H, 2.97; N, 4.87.

Selected crystal data of 3: $C_{39}H_{29}Cl_2F_3IrN_3P_2$; M = 921.69; monoclinic; space group = $P2_1/c$; *a* = 12.5887(7) Å, *b* = 11.3322(7) Å, *c* = 25.3533(14) Å, β = 96.5926(15)°, *V* = 3592.9(4) $Å^3$; *Z* = 4; ρ_{calcd} = 1.704 $Mg \cdot m^{-3}$; *F*(000) = 1808; crystal size = 0.20 × 0.15 × 0.05 mm^3; λ(Mo-Kα) = 0.71073 Å; T = 150(2) K; μ = 4.003 mm^{-1}; 20453 reflections collected, 8229 independent reflections (R_{int} = 0.0325), GOF = 1.046, final $R_1[I > 2\sigma(I)]$ = 0.0298 and wR_2(all data) = 0.0564.

Preparation of [**Ir(dppBz)(fppz)(bipz)] (4)**: A mixture of **3** (145 mg, 0.16 mmol) and $bipzNa_2$ (99 mg, 0.31 mmol) in 20 mL of anhydrous DMF was refluxed for 12 h.

After removal of solvent, the residue was purified by silica gel column chromatography using a 1:3 mixture of hexane and CH_2Cl_2 as the eluent. Crystallization from hexane and CH_2Cl_2 at RT gave white crystals (**4**, 72 mg, 0.06 mmol, 41%).

Data for 4: MS (FAB, ^{192}Ir): *m/z* 1119 [M^+]; ^{1}H NMR (500 MHz, CD_2Cl_2, 294 K): δ 7.93 (d, *J* = 7.7 Hz, 1H), 7.91 (d, *J* = 7.7 Hz, 1H), 7.80 ~ 7.63 (m, 7H), 7.52 (t, *J* = 7.4 Hz, 1H), 7.45 (t, *J* = 7.9 Hz, 2H), 7.40 (td, J = 7.7, 2.6 Hz, 2H), 7.27 (td, J = 7.7, 2.6 Hz, 2H), 7.18 (t, *J* = 7.4 Hz, 1H), 7.15 (t, J = 7.4 Hz, 1H), 6.89 ~ 6.78 (m, 6H), 6.65 (d, *J* = 7.7 Hz, 1H), 6.63 (d, *J* = 7.7 Hz, 1H), 6.58 (s, 1H) , 6.51 (d, *J* = 7.7 Hz, 1H), 6.48 (d, *J* = 7.7 Hz, 1H), 6.10 (s, 1H), 6.07 (s, 1H). ^{19}F NMR (470 MHz, CD_2Cl_2, 294 K): δ -60.88 (s, 3F), -61.23 (s, 3F), -61.57 (s, 3F). ^{31}P NMR (202 MHz, CD_2Cl_2, 294 K): δ 15.99 (d, J_{PP} = 3.1 Hz, 1P), 15.24 (d, J_{PP} = 3.1 Hz, 1P). Anal. Calcd. for $C_{47}H_{31}F_9IrN_7P_2$: C, 50.45; H, 2.79; N, 8.76. Found: C, 50.81; H, 3.05; N, 8.61.

Selected crystal data of 4: $C_{47.5}H_{32}ClF_9IrN_7P_2$; M = 1161.39; tetragonal; space group = I-4; *a* = 27.4183(6) Å, *b* = 27.4183(6) Å, *c* = 11.5349(4) Å, *V* = 8671.5(4) Å^3; *Z* = 8; ρ_{calcd} = 1.779 Mg·m^{-3}; *F*(000) = 4568; crystal size = 0.33 × 0.15 × 0.15 mm^3; λ(Mo-Kα) = 0.71073 Å; T = 150(2) K; μ = 3.300 mm^{-1}; 33645 reflections collected, 9955 independent reflections (R_{int} = 0.0538), GOF = 0.924, final $R_1[I > 2\sigma(I)]$ = 0.0296 and wR_2(all data) = 0.0591.

Preparation of [Ir(dppBz)(fppz)(mepz)] (5): This was prepared using a procedure similar to that described for **4**. Crystallization from hexane and CH_2Cl_2 at RT gave white crystals (154 mg, 0.13 mmol, 49%).

Data for 5: MS (FAB, ^{192}Ir): *m/z* 1161 [M^+]; ^{1}H NMR (400 MHz, CD_2Cl_2, 294 K): δ 8.34 (d, *J* = 11.4 Hz, 1H), 8.33 (d, *J* = 11.4 Hz, 1H), 7.84 (d, *J* = 8.2 Hz, 1H), 7.68 ~ 7.55 (m, 6H), 7.46 ~ 7.38 (m, 5H), 7.18 ~ 7.12 (m, 3H), 7.03 (t, *J* = 7.3 Hz, 1H), 6.96 (d, *J* = 10.6 Hz, 1H), 6.94 (d, *J* = 11.0 Hz, 1H), 6.84 (t, *J* = 7.8 Hz, 2H), 6.76 (t, *J* = 7.8 Hz, 2H), 6.72 (s, 1H), 6.64 (t, *J* = 6.6 Hz, 1H), 6.55 ~ 6.53 (m, 1H), 6.29 (d, *J* =11.4 Hz, 1H), 6.27 (d, *J* = 11.4 Hz, 1H), 6.09 (s, 1H), 5.89 (s, 1H), 0.88 (s, 3H) , 0.81 (s, 3H). ^{19}F NMR (470 MHz, CD_2Cl_2, 294 K): δ -60.99 (s, 3F), -60.46 (s, 3F), -61.47 (s, 3F). ^{31}P NMR (202 MHz,

CD_2Cl_2, 294 K): δ 16.83 (d, J_{PP} = 4.8 Hz, 1P), 10.14 (d, J_{PP} = 4.8 Hz, 1P). Anal. Calcd. for $C_{50}H_{37}F_9IrN_2P_2$: C, 51.72; H, 3.21; N, 8.44. Found: C, 51.80; H, 3.05; N, 8.47.

Selected crystal data of 5: $C_{57}H_{52}F_9IrN_7O_2P_2$; M = 1292.19; triclinic; space group = *P*-1; *a* = 12.1776(5) Å, *b* = 14.1050(6) Å, *c* = 16.7979(7) Å, α = 96.1636(9)°, β = 109.7611(8)°, γ = 91.3795(8)°, *V* = 2694.1(2) Å^3; *Z* = 2; ρ_{calcd} = 1.593 Mg·m^{-3}; *F*(000) = 1294; crystal size = 0.25 × 0.25 × 0.10 mm^3; λ(Mo-Kα) = 0.71073 Å; T = 200(2) K; μ = 2.619 mm^{-1}; 35150 reflections collected, 12333 independent reflections (R_{int} = 0.0441), GOF = 1.053, final $R_1[I > 2\sigma(I)]$ = 0.0390 and wR_2(all data) = 0.0973.

Preparation of [Ir(dppBz)(fppz)(bipzH)H] (6): A DGME solution of **3** (100 mg, 0.11 mmol) and $bipzNa_2$ (68 mg, 0.22 mmol) was heat at 190°C for 12 h. After removal of solvent, the residue was purified by silica gel column chromatography using a 1:3 mixture of hexane and CH_2Cl_2 as the eluent. Crystallization from hexane and CH_2Cl_2 at RT gave colorless **6** (57 mg, 0.05 mmol, 47%).

Data for 6: MS (FAB, ^{192}Ir): *m*/*z* 1121 [M$^+$]; ^{1}H NMR (500 MHz, CD_2Cl_2, 294 K): δ 14.85 (s, 1H), 8.05 ~ 8.01 (m, 2H), 7.72 (d, *J* = 10.8 Hz, 1H), 7.71 (d, *J* = 10.8 Hz, 1H), 7.60 (t, *J* = 7.6 Hz, 1H), 7.55 ~ 7.48 (m, 5H), 7.46 ~ 7.40 (m, 3H), 7.33 (d, *J* = 7.0 Hz, 3H), 7.14 ~ 7.09 (m, 4H), 7.04 (t, *J* = 7.5 Hz, 1H), 6.84 (t, *J* = 7.8 Hz, 2H), 6.74 (s, 1H), 6.41 ~ 6.37 (m, 3H), 6.16 (t, *J* = 6.1 Hz, 1H), 6.15 (s, 1H), 6.06 (s, 1H), -18.69 (dd, J_{HP} = 23.6, 16.3 Hz, 1H). ^{19}F NMR (470 MHz, CD_2Cl_2, 294 K): δ -61.43 (s, 3F), -61.77 (s, 3F), -62.08 (s, 3F). ^{31}P NMR (202 MHz, CD_2Cl_2, 294 K): δ 28.36 (d, J_{HP} = 16.3 Hz, 1P), 24.26 (d, J_{HP} = 23.6 Hz, 1P). Anal. Calcd. for $C_{47}H_{31}F_9IrN_7P_2$: C, 50.36; H, 2.97; N, 8.75. Found: C, 49.98; H, 2.85; N, 8.89.

Selected crystal data of 6: $C_{47}H_{33}F_9IrN_7P_2$; M = 1120.94; triclinic; space group = *P*-1; *a* = 12.3245(6) Å, *b* = 12.3928(6) Å, *c* = 15.3788(7) Å, α = 85.5453(12)°, β = 87.6200(10)°, γ = 72.6127(10)°, *V* = 2234.37(18) Å^3; *Z* = 2; ρ_{calcd} = 1.666 Mg·m^{-3}; *F*(000) = 1104; crystal size = 0.22 × 0.20 × 0.17 mm^3; λ(Mo-Kα) = 0.71073 Å; T = 150(2) K; μ = 3.140 mm^{-1}; 29231 reflections collected, 10209 independent reflections (R_{int} = 0.0455), GOF = 1.026, final $R_1[I > 2\sigma(I)]$ = 0.0324 and wR_2(all data) = 0.0700.

Conversion of [Ir(dppBz)(fppz)(bipzH)H] (6) to [Ir(dppBz)(fppz)(bipz)] (4). A solution of **6** (50 mg, 0.04 mmol) and K_2CO_3 (18 mg, 0.13 mmol) in DMF (10 mL) was refluxed for 24 hr. The solvent was evaporated and the residue was purified by silica gel column chromatography using a 1:3 mixture of hexane and CH_2Cl_2 as the eluent. Crystallization from hexane and CH_2Cl_2 at RT gave white crystals (**4**, 12 mg, 0.01 mmol, 25%).

Computational studies: Calculations were performed with the Gaussian 09 package[27] using the DFT-wave hybrid B3LYP functional,[28] the LANL2DZ pseudopotential for iridium[29] and the basis set 6-31G** for all other atoms.[30] The default polarization continuum model PCM[31] with CH_2Cl_2 as solvent was applied in all cases. The optimized geometries were confirmed as true minima by the absence of imaginary frequencies from frequency calculations. Good agreements were found for bond lengths and bond angles between geometries of **2** - **6** calculated at B3LYP/LANL2DZ:6-31G**/PCM and determined by X-ray crystallography, giving confidence in the use of the B3LYP/LANL2DZ:6-31G**/PCM model chemistry for Ir(III) metal complexes here (Table S4). The computed bond lengths involving iridium are consistently longer (0.02 - 0.06 Å) than experimental distances as expected, while the bond angles are almost identical in both geometries with differences of less than three degrees. This model chemistry has been used elsewhere on related complexes **A** and **B** where other model chemistries such as pure DFT and pure wave methods gave similar results.[8] Here, the model chemistry B3LYP-GD3/LANL2DZ:6-31G**/PCM incorporating the recently popular Grimme empirical dispersion model (GD3)[32] were also examined on **2** - **6** which gave similar data. Using much larger basis sets, 6-311+G** instead of 6-31G** gave virtually identical results.

Electronic structure calculations on Ir(III) complexes **2** - **6** were carried out to compare their molecular orbital energies and compositions (Tables S1 and S2) with observed electrochemical and photophysical data. Data from electronic structure calculations were analyzed further with GaussSum[33] (Tables 2, S1-S3). The orbital plots were plotted at ±0.065 $(e/bohr^3)^{½}$ with GabEdit[34] with hydrogen atoms omitted for clarity (Figures 7 and 8).

TD-DFT computations were carried out on the optimized ground state S_0 geometries of **2** - **6** to predict their absorption data (Table 2) with 25 triplet and 25 singlet states calculated. The oscillator strengths (*f*) from $S_0 \rightarrow T_n$ transitions could not be calculated with current TD-DFT methods. The predicted $S_0 \leftarrow T_1$ emission wavelengths were converted from the TD-DFT absorption wavelengths of $S_0 \rightarrow T_1$ on the optimized S_0 geometries using an energy scaling factor of 0.94 to take into account the expected constant Stokes shift in the Ir(III) complexes.[35] Simple scaling factors have been used in many other computational studies to compare with experimental data especially for infrared[36] and NMR chemical shift data.[37]

Supporting information. Electrochemical, photophysical, X-ray structural determination and OLED fabrication procedures are described along with ^1H and ^{31}P NMR spectra, additional absorption, electrochemical and computational data (geometry parameters, MO energies, orbital contributions, cartesian coordinates, predicted new Ir(III) complexes). CIF data of Ir(III) complexes **2** - **6** (cf. CCDC 1525321-1525325).

Acknowledgments. This work was supported by the Ministry of Science and Technology of Taiwan, under the grant number MOST 105-2811-M-007-028.

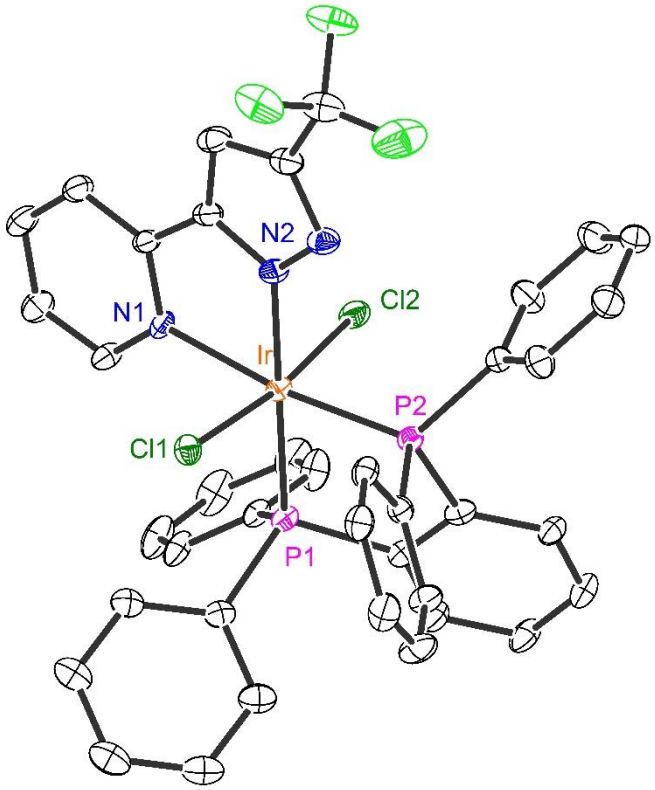

Figure 1. Crystal structure of **2** with thermal ellipsoids shown at 30% probability level. Selected bond distances: Ir-N(1) = 2.139(3), Ir-N(2) = 2.058(4), Ir-P(1) = 2.3057(12), Ir-P(2) = 2.2773(12), Ir-Cl(1) = 2.3548(11), and Ir-Cl(2) = 2.3661(12) Å; selected angles: N(1)-Ir-N(2) = 77.22(15), P(1)-Ir-P(2) = 83.97(4) and Cl(1)-Ir-Cl(2) = 172.59(4)°. Hydrogen atoms and diethyl ether solvate are omitted for clarity.

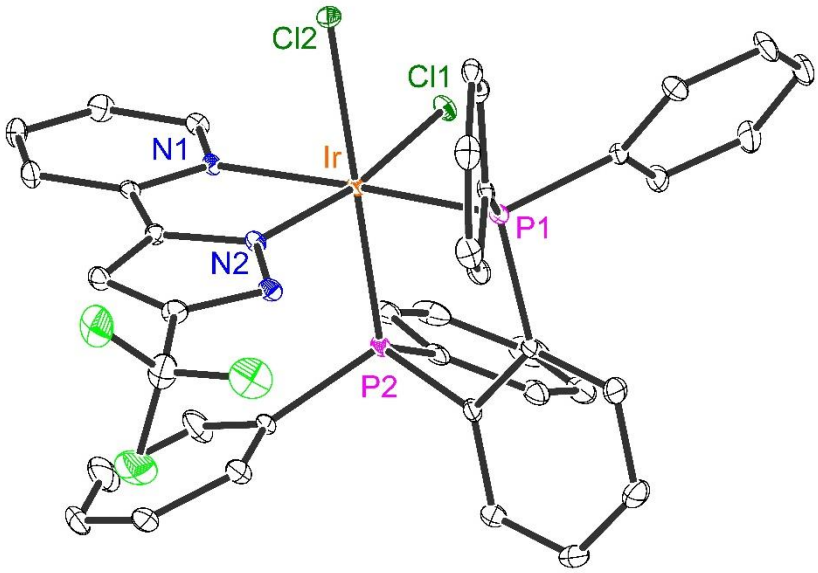

Figure 2. Crystal structure of **3** with thermal ellipsoids shown at 30% probability level. Selected bond distances: Ir-N(1) = 2.147(3), Ir-N(2) = 2.021(3), Ir-P(1) = 2.2831(9), Ir-P(2) = 2.2544(8), Ir-Cl(1) = 2.3648(8), and Ir-Cl(2) = 2.4240(8) Å; selected angles: N(1)-Ir-N(2) = 77.60(11), P(1)-Ir-P(2) = 85.74(3) and Cl(1)-Ir-Cl(2) = 87.84(3)°. Hydrogen atoms are omitted for clarity.

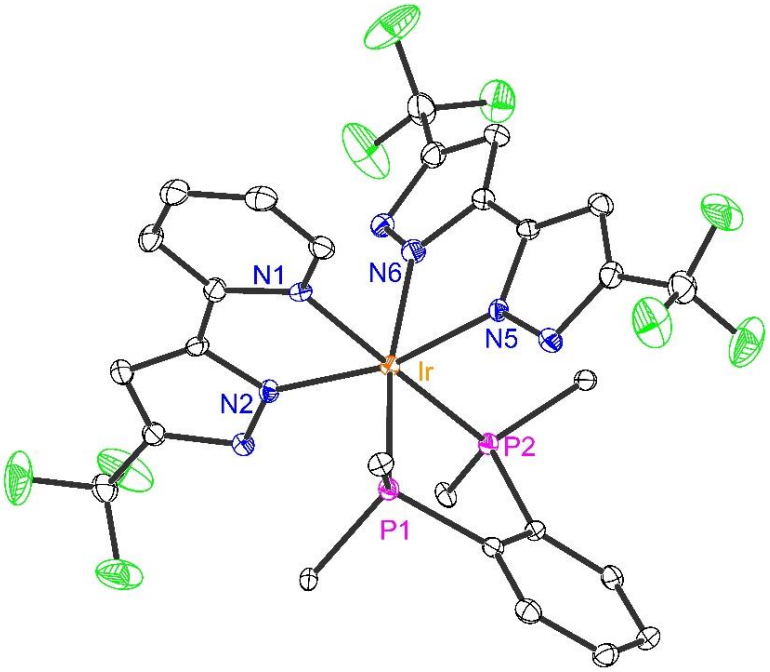

Figure 3. Crystal structure of complex **4** with thermal ellipsoids shown at 30% probability level; only the ipso-carbons of four phenyl groups of dppBz chelates are shown for clarity. Hydrogen atoms and dichloromethane solvate are also omitted for clarity. Selected bond distances: Ir-N(1) = 2.121(5), Ir-N(2) = 2.047(5), Ir-N(5) = 2.047(5), Ir-N(6) = 2.091(5), Ir-P(1) = 2.2914(14), and Ir-P(2) = 2.2699(16) Å; selected angles: N(1)-Ir-N(2) = 77.3(2), N(5)-Ir-N(6) = 77.07(19) and P(1)-Ir-P(2) = 85.45(6)°.

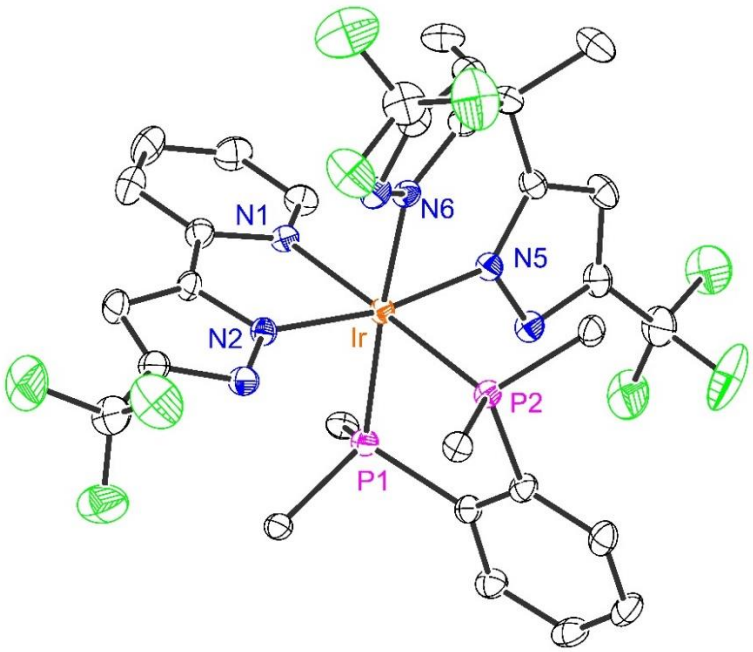

Figure 4. Crystal structure of complex **5** with thermal ellipsoids shown at 30% probability level; only the ipso-carbons of four phenyl groups of dppBz chelates are shown for clarity. Hydrogen atoms and solvates such as ethyl acetate and hexane molecules are also omitted for clarity. Selected bond distances: Ir-N(1) = 2.113(3), Ir-N(2) = 2.044(3), Ir-N(5) = 2.056(3), Ir-N(6) = 2.096(3), Ir-P(1) = 2.3007(10), and Ir-P(2) = 2.2860(10) Å; selected angles: N(1)-Ir-N(2) = 77.65(13), N(5)-Ir-N(6) = 85.53(13) and P(1)-Ir-P(2) = 84.50(4)°.

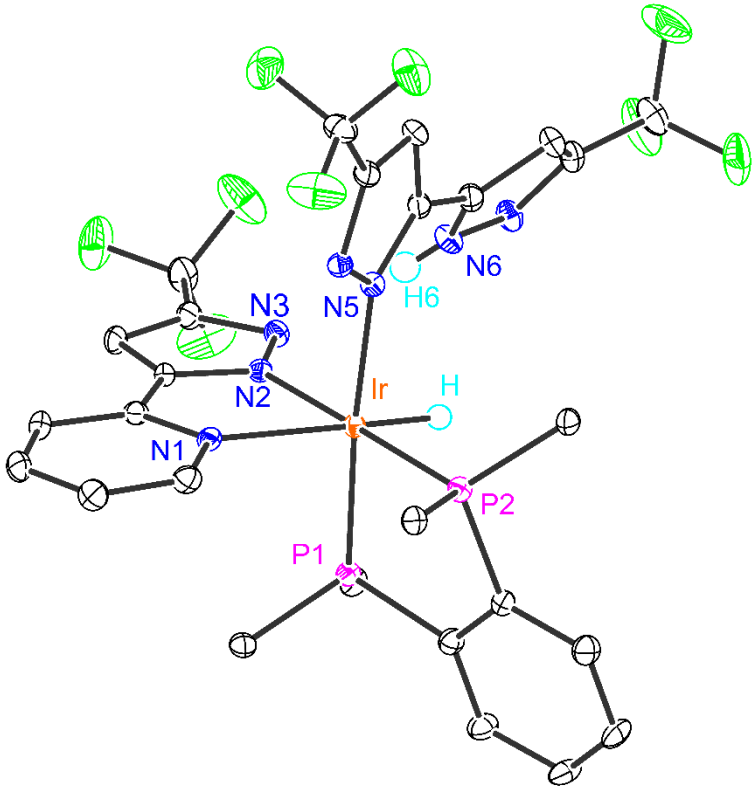

Figure 5. Crystal structure of **6** with thermal ellipsoids shown at 30% probability level; only the *ipso*-carbons of four phenyl groups of dppBz chelates were shown for clarity. Selected distances: Ir-N(1) = 2.222(3), Ir-N(2) = 2.070(3), Ir-N(5) = 2.111(3), Ir-P(1) = 2.2488(9), Ir-P(2) = 2.2623(9), Ir-H = 1.43(3), N(6)-H(6) = 0.75(4) and N(3)···H(6) = 2.02(4) Å; selected angles: N(1)-Ir-N(2) = 74.94(10), N(5)-Ir-H = 90.9(13) and P(1)-Ir-P(2) = 85.97(3)°.

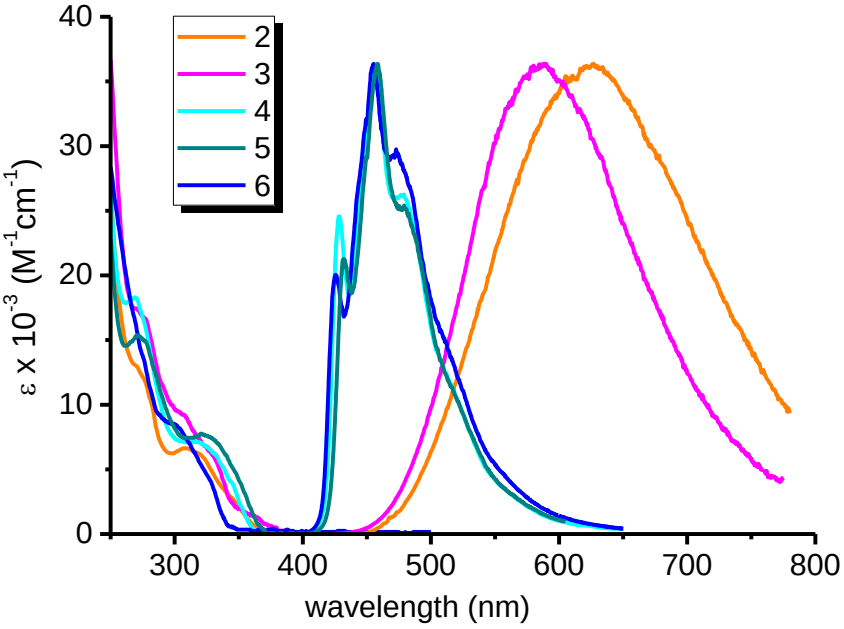

Figure 6. UV-Vis absorption spectra in CH_2Cl_2 (10^{-5} M) and solid state emission spectra of Ir(III) complexes **2** - **6** as powders measured at RT.

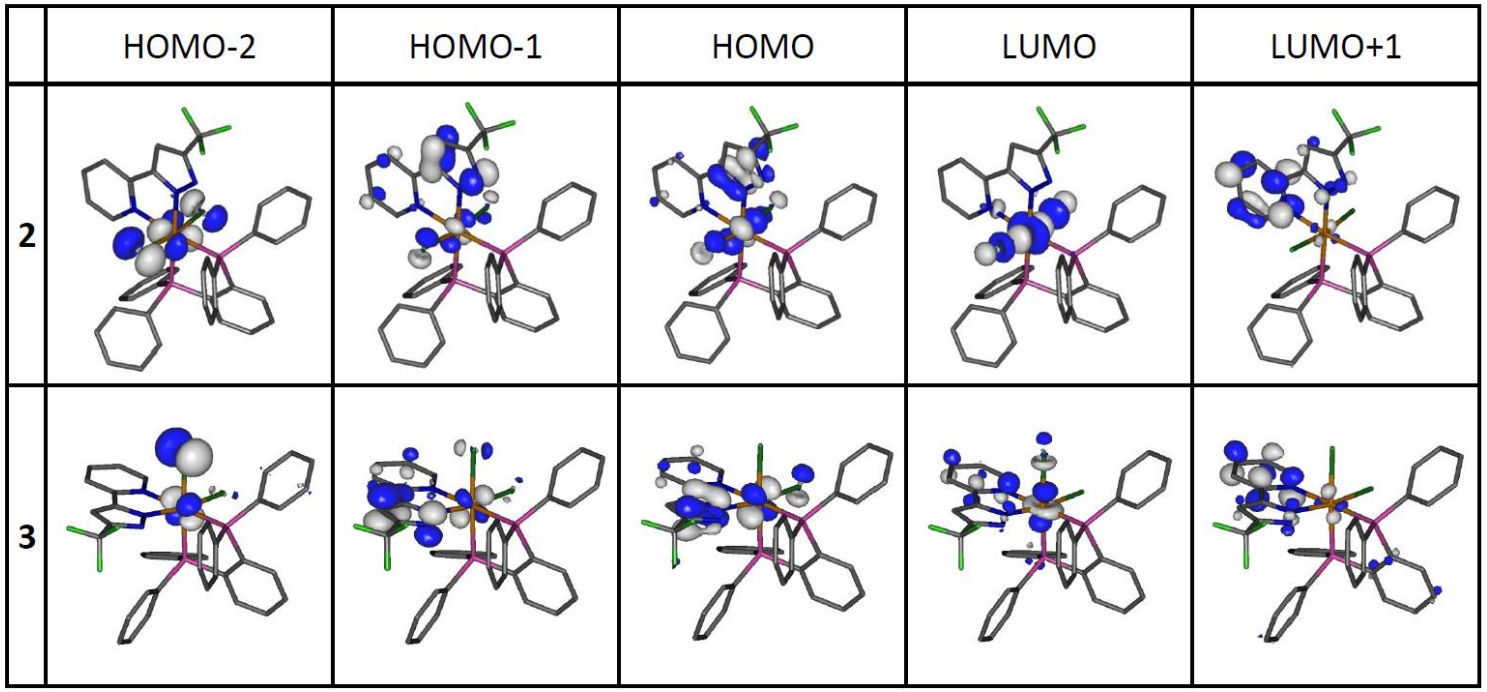

Figure 7. Plots of important orbitals for Ir(III) complexes **2** and **3**.

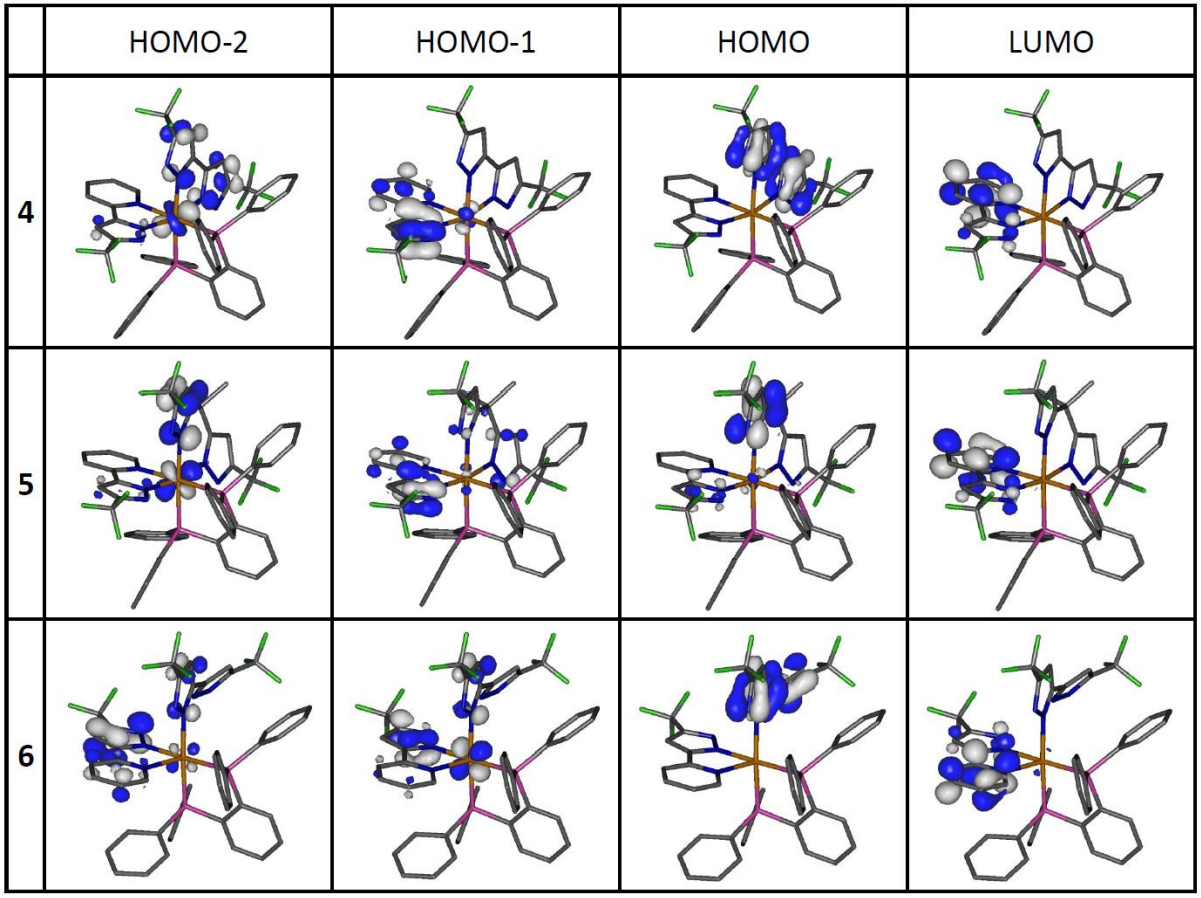

Figure 8. Plots of important orbitals for Ir(III) complexes **4** - **6**.

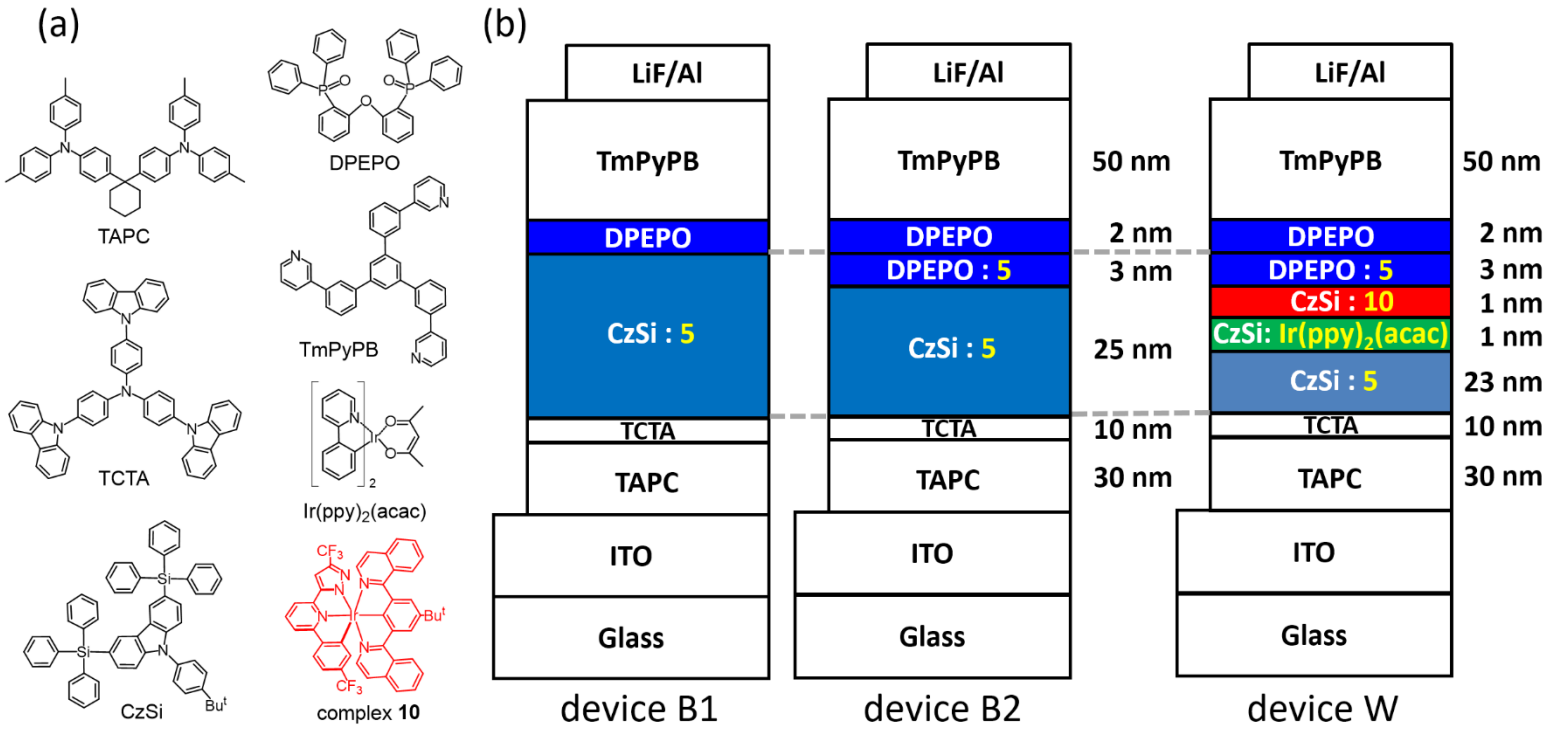

Figure 9. (a) Molecular structures of the materials used and (b) schematic structures of the tested blue and white OLEDs.

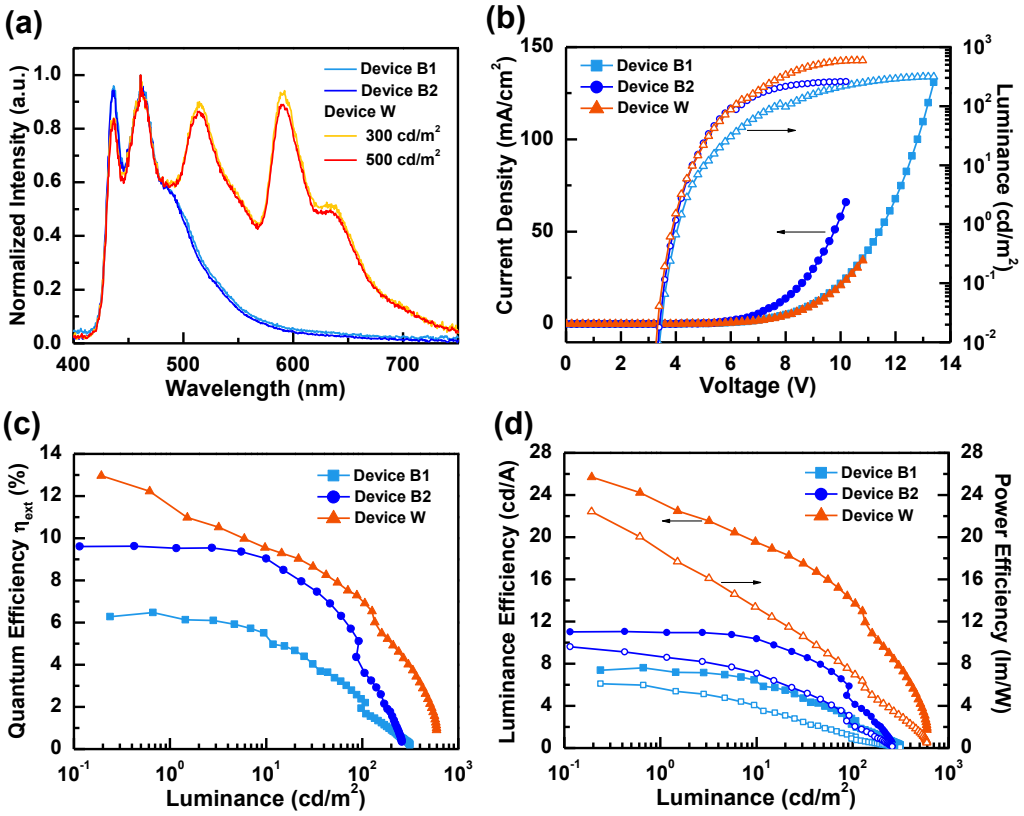

Figure 10. (a) EL spectra of devices B1, B2 and W, (b) current density-voltage-luminance (*J-V-L*) characteristics, (c) external quantum efficiency *vs*. luminance, (d) power efficiencies/luminance efficiencies *vs*. luminance for devices B1, B2 and W.

Table 1. Selected photophysical and electrochemical properties of the studied Ir(III) complexes.

	Photophysical data					Electrochemical data	
	abs. λ_{max} (nm) [ε (10^{-3} $M^{-1}cm^{-1}$)][a]	PL λ_{max} (nm)[b]	Q.Y. (%)[b]	τ_{obs} (µs)[c]	k_r (10^4 s^{-1})[c]	E_{pa}^{ox} (V)[d]	E_{pc}^{red} (V)[d]
2	269 [13.0], 308 [6.6]	627; [630]	10; [11]	2.8	3.6	1.23	-2.20
3	271 [17.3], 308 [9.1], 352 [1.9]	590; [592]	90; [47]	3.8	24	1.23	-2.27
4	268 [18.2], 317[7.1]	428, 456, 479; [429, 455, 479]	51; [27]	51	1.0	0.96	-2.64
5	271 [15.4], 321 [7.7]	431, 458, 479; [432, 459, 480]	70; [54]	53	1.3	1.19	-2.63
6	298 [8.5]	425, 455, 473; [420, 448, 466]	69; [58]	75	0.92	1.19	-2.60

[a] UV-Vis spectra were recorded in CH_2Cl_2 at a conc. of 10^{-5} M.

[b] PL data of the neat powder and PMMA films (5 wt.%) are depicted in standard text format and enclosed in square brackets, respectively.

[c] Data measured in powder and $k_r = \Phi/\tau_{obs}$.

[d] E_{pa} and E_{pc} are the anodic and cathodic peak potentials respectively and referenced to the FcH^+/FcH couple. The oxidation and reduction experiments were conducted in CH_2Cl_2 and THF solution, respectively.

Table 2. Calculated photophysical data for **2** – **6**. Observed photophysical data are included for comparison.

	Calculated absorption state and MO transitions[a]	Nature of transitions[b]	Metal contributions[c]	Oscillator strength (*f*)	Absorption calculated (nm)	Absorption observed[d] (nm)	Emission calculated[e] (nm)	Emission observed[f] (nm)	Stokes shift calculated[g] (cm^{-1})	Stokes shift observed[h] (cm^{-1})
2	$S_0 \rightarrow T_1$ (H→ L 66%)	^{3}MX → MX	27 → 43	–	501		533	627	11000	13460
	$S_0 \rightarrow S_1$ (H → L 71%)	^{1}MX → MX	28 → 43	0.0003	419	380 (edge)				
	$S_0 \rightarrow S_3$ (H → L+1 80%)	^{1}MX → L	30 → 7	0.0101	336	340				
3	$S_0 \rightarrow T_1$ (H → L 57%)	^{3}MX → ML	25 → 19	–	416		442	590	7490	11060
	$S_0 \rightarrow S_1$ (H → L 58%)	^{1}MX → ML	26 → 19	0.0028	379	410 (edge)				
	$S_0 \rightarrow S_2$ (H-2→ L 21%)	^{1}MX → ML	23 → 23	0.0103	332	357				
4	$S_0 \rightarrow T_1$ (H-1→ L 73%)	^{3}(M)L → L’	8 → 2	–	406		432	428	8100	6400
	$S_0 \rightarrow S_1$ (H → L 98%)	^{1}(M)L → L’	2 → 2	0.0008	377	380 (edge)				
	$S_0 \rightarrow S_4$ (H-1 → L 69%)	^{1}(M)L → L’	7 → 2	0.0500	320	336				
5	$S_0 \rightarrow T_1$ (H-1 → L 52%)	^{3}(M)L → L’	5 → 2	–	410		436	431	8020	5130
	$S_0 \rightarrow S_1$ (H → L 89%)	^{1}(M)L → L’	5 → 2	0.0220	330	380 (edge)				
	$S_0 \rightarrow S_2$ (H-2 → L 42%)	^{1}ML → L’	18 → 4	0.0477	323	353				
6	$S_0 \rightarrow T_1$ (H-2 → L 44%)	^{3}ML → L’	14 → 3	–	392		417	425	7970	7340
	$S_0 \rightarrow S_1$ (H→L 94%)	^{1}(M)L → L’	3 → 3	0.0053	323	355 (edge)				
	$S_0 \rightarrow S_2$ (H-1→L 83%)	^{1}ML → L’	22 → 3	0.0428	313	324				

[a] H = HOMO, L = LUMO.

[b] ^{3}MX $\rightarrow$ MX = triplet mixed metal-chloride to metal-chloride transition, ^{1}MX $\rightarrow$ MX = singlet mixed metal-chloride to metal-chloride transition, ^{3}MX $\rightarrow$ ML = triplet mixed metal chloride to mixed metal ligand transition, ^{3}(M)L $\rightarrow$ L' = triplet ligand containing minor metal contribution to other ligand transition, ^{3}ML $\rightarrow$ L' = triplet mixed metal-ligand to other ligand transition.
[c] Iridium atom contribution as percentage (%) of state.
[d] Observed lowest energy absorption maxima were obtained from Gaussian deconvolution analyses of the absorption spectra (Figures S3 - S7) along with lowest energy band edge values (Figure S1).
[e] Calculated $S_0 \leftarrow T_1$ from calculated $S_0 \rightarrow T_1$ values with an energy scaling factor.
[f] Highest energy band observed.
[g] Energies calculated from difference in energy between low energy $S_0 \rightarrow S_n$ transition of high oscillator strength ($f > 0.01$) and $S_0 \leftarrow T_1$.
[h] Energies calculated from difference in energy between lowest energy observed absorption maximum and observed highest energy emission maximum.

Table 3. EL Characteristics of OLEDs with different EML structures.

Device	EQE (%)		LE (cd/A)		PE (lm/W)		V_{on} (V)CRI [Ra]/CCT (K)		CIE1931 (x, y)	
	[a]	[b]	[a]	[b]	[a]	[b]	[c]	[d]	[b]	[d]
B1	6.5	2.3	7.6	2.7	6.1	1.1	4.1	—	0.16, 0.16	0.18, 0.18
B2	9.6	3.8	11.0	4.4	9.6	2.2	4.0	—	0.16, 0.15	0.18, 0.18
W	13.0	7.0	25.7	14.0	22.4	7.2	3.9	90.7/5943	0.35, 0.36	0.32, 0.34

[a] Maximum efficiencies. [b] Data measured at a brightness of 100 cd/m^2. [c] Turn-on voltage measured at 1 cd/m^2. [d] Data recorded at 300 cd/m^2.

References

[1] a) S. Ladouceur, E. Zysman-Colman, *Eur. J. Inorg. Chem.* **2013**, *2013*, 2985-3007; b) N. Darmawan, C.-H. Yang, M. Mauro, R. Frohlich, L. De Cola, C.-H. Chang, Z.-J. Wu, C.-W. Tai, *J. Mater. Chem. C* **2014**, *2*, 2569-2582; c) A. F. Henwood, E. Zysman-Colman, *Chem. Commun.* **2017**, *53*, 807-826; d) D. Ma, T. Tsuboi, Y. Qiu, L. Duan, *Adv. Mater.* **2017**, *29*, 1603253.

[2] a) Q. Zhao, F. Li, C. Huang, *Chem. Soc. Rev.* **2010**, *39*, 3007-3030; b) K. M.-C. Wong, V. W.-W. Yam, *Acc. Chem. Res.* **2011**, *44*, 424-434; c) G. Zhou, W.-Y. Wong, X. Yang, *Chem. Asian J.* **2011**, *6*, 1706-1727; d) E. Baggaley, J. A. Weinstein, J. A. G. Williams, *Coord. Chem. Rev.* **2012**, *256*, 1762-1785; e) Y. You, W. Nam, *Chem. Soc. Rev.* **2012**, *41*, 7061-7084; f) X. Zhang, Z. Chi, Y. Zhang, S. Liu, J. Xu, *J. Mater. Chem. C* **2013**, *1*, 3376-3390; g) W. C. H. Choy, W. K. Chan, Y. Yuan, *Adv. Mater.* **2014**, *26*, 5368-5399; h) G. Li, J. Lin, *Chem. Soc. Rev.* **2014**, *43*, 7099-7131; i) X. Yang, X. Xu, G. Zhou, *J. Mater. Chem. C* **2015**, *3*, 913-944.

[3] a) Y. Wang, S. Wang, S. Shao, J. Ding, L. Wang, X. Jing, F. Wang, *Dalton Trans.* **2015**, *44*, 1052-1059; b) Y. Wang, S. Wang, N. Zhao, B. Gao, S. Shao, J. Ding, L. Wang, X. Jing, F. Wang, *Polym. Chem.* **2015**, *6*, 1180-1191.

[4] A total of 1569 structures of tris-bidentate iridium complexes were found in a Cambridge Structural Database search using Conquest 1.19 on CSD version 5.38.

[5] There are 412, 174, 34, 27, 50 and 39 crystal structures of tris-bidentate iridium complexes containing ppy, F2ppy, ppz, F2ppz, bpy and dtbbpy ligands respectively found by conquest searches on CSD version 5.38 database.

[6] a) A. B. Tamayo, B. D. Alleyne, P. I. Djurovich, S. Lamansky, I. Tsyba, N. N. Ho, R. Bau, M. E. Thompson, *J. Am. Chem. Soc.* **2003**, *125*, 7377-7387; b) T. Sajoto, P. I. Djurovich, A. Tamayo, M. Yousufuddin, R. Bau, M. E. Thompson, R. J. Holmes, S. R. Forrest, *Inorg. Chem.* **2005**, *44*, 7992-8003; c) Y. Chi, P.-T. Chou, *Chem. Soc. Rev.* **2010**, *39*, 638-655.

[7] P.-T. Chou, Y. Chi, M.-W. Chung, C.-C. Lin, *Coord. Chem. Rev.* **2011**, *255*, 2653-2665.

[8] J.-L. Liao, Y. Chi, Z.-T. Sie, C.-H. Ku, C.-H. Chang, M. A. Fox, P. J. Low, M.-R. Tseng, G.-H. Lee, *Inorg. Chem.* **2015**, *54*, 10811-10821.

[9] Y. Chi, K.-L. Wu, T.-C. Wei, *Chem. Asian J.* **2015**, *10*, 1098-1115.

[10] C.-H. Lin, C.-Y. Lin, J.-Y. Hung, Y.-Y. Chang, Y. Chi, M.-W. Chung, Y.-C. Chang, C. Liu, H.-A. Pan, G.-H. Lee, P.-T. Chou, *Inorg. Chem.* **2012**, *51*, 1785-1795.

[11] a) Y. Chi, B. Tong, P.-T. Chou, *Coord. Chem. Rev.* **2014**, *281*, 1-25; b) C.-W. Lu, Y. Wang, Y. Chi, *Chem. Eur. J.* **2016**, *22*, 17892-17908.

[12] a) M. S. Lowry, W. R. Hudson, R. A. Pascal, S. Bernhard, *J. Am. Chem. Soc.* **2004**, *126*, 14129-14135; b) A. S. Ionkin, Y. Wang, W. J. Marshall, V. A. Petrov, *J. Organomet. Chem.* **2007**, *692*, 4809-4827; c) Y. Jian, S. Peng, X. Li, X. Wen, J. He, L. Jiang, Y. Dang, *Inorg. Chim. Acta* **2011**, *368*, 37-43; d) E. C. Constable, C. E. Housecroft, E. Schönhofer, J. Schönle, J. A. Zampese, *Polyhedron* **2012**, *35*, 154-160; e) S.-X. Luo, L. Wei, X.-H. Zhang, M. H. Lim, K. X. V. Lin, M. H. V. Yeo, W.-H. Zhang, Z.-P. Liu, D. J. Young, T. S. A. Hor, *Organometallics* **2013**, *32*, 2908-2917; f) P. Alam, I. R. Laskar, C. Climent, D. Casanova, P. Alemany, M. Karanam, A. R. Choudhury, J. Raymond Butcher, *Polyhedron* **2013**, *53*, 286-294; g) E. A. Katlenok, A. A. Zolotarev, K. P. Balashev, *Russ. J. Gen. Chem.* **2016**, *86*, 2508-2514; h) Y. Takahira, E. Murotani, K. Fukuda, V. Vohra, H. Murata, *J. Fluorine Chem.* **2016**, *181*, 56-60; i) D. Rota Martir, A. K. Bansal, V. Di Mascio, D. B. Cordes, A. F. Henwood, A. Slawin, P. Kamer, L. Martinez-Sarti, A. Pertegas, H. J. Bolink, I. Samuel, E. Zysman-Colman, *Inorg. Chem. Front.* **2016**, *3*, 218-235.

[13] C.-H. Lin, Y.-C. Chiu, Y. Chi, Y.-T. Tao, L.-S. Liao, M.-R. Tseng, G.-H. Lee, *Organometallics* **2012**, *31*, 4349-4355.

[14] a) E. Baranoff, S. Suarez, P. Bugnon, C. Barolo, R. Buscaino, R. Scopelliti, L. Zuppiroli, M. Grätzel, M. K. Nazeeruddin, *Inorg. Chem.* **2008**, *47*, 6575-6577; b) J.-Y. Hung, Y. Chi, I. H. Pai, Y.-C. Yu, G.-H. Lee, P.-T. Chou, K.-T. Wong, C.-C. Chen, C.-C. Wu, *Dalton Trans.* **2009**, 6472-6475; c) B.-S. Du, C.-H. Lin, Y. Chi, J.-Y. Hung, M.-W. Chung, T.-Y. Lin, G.-H. Lee, K.-T. Wong, P.-T. Chou, W.-Y. Hung, H.-C. Chiu, *Inorg. Chem.* **2010**, *49*, 8713-8723.

[15] a) F.-C. Hsu, Y.-L. Tung, Y. Chi, C.-C. Hsu, Y.-M. Cheng, M.-L. Ho, P.-T. Chou, S.-M. Peng, A. J. Carty, *Inorg. Chem.* **2006**, *45*, 10188-10196; b) Y.-C. Chiu, C.-H. Lin, J.-Y. Hung, Y. Chi, Y.-M. Cheng, K.-W. Wang, M.-W. Chung, G.-H. Lee, P.-T. Chou, *Inorg. Chem.* **2009**, *48*, 8164-8172.

[16] a) A. F. Rausch, L. Murphy, J. A. G. Williams, H. Yersin, *Inorg. Chem.* **2012**, *51*, 312-319; b) B.-S. Du, J.-L. Liao, M.-H. Huang, C.-H. Lin, H.-W. Lin, Y. Chi, H.-A. Pan, G.-L. Fan, K.-T. Wong, G.-H. Lee, P.-T. Chou, *Adv. Funct. Mater.* **2012**, *22*, 3491-3499.

[17] a) S.-J. Su, C. Cai, J. Kido, *J. Mater. Chem.* **2012**, *22*, 3447-3456; b) S. O. Jeon, J. Y. Lee, *J. Mater. Chem.* **2012**, *22*, 4233-4243; c) H.-H. Kuo, Y.-T. Chen, L. R. Devereux, C.-C. Wu, M. A. Fox, C.-Y. Kuei, Y. Chi, G.-H. Lee, *Adv. Mater.* **2017**, *29*, 1702464.

[18] a) C.-H. Yang, Y.-M. Cheng, Y. Chi, C.-J. Hsu, F.-C. Fang, K.-T. Wong, P.-T. Chou, C.-H. Chang, M.-H. Tsai, C.-C. Wu, *Angew. Chem. Int. Ed.* **2007**, *46*, 2418-2421;

b) C.-H. Chang, Z.-J. Wu, C.-H. Chiu, Y.-H. Liang, Y.-S. Tsai, J.-L. Liao, Y. Chi, H.-Y. Hsieh, T.-Y. Kuo, G.-H. Lee, H.-A. Pan, P.-T. Chou, J.-S. Lin, M.-R. Tseng, *ACS Appl. Mater. Interfaces* **2013**, *5*, 7341-7351.

[19] a) M.-H. Tsai, H.-W. Lin, H.-C. Su, T.-H. Ke, C.-C. Wu, F.-C. Fang, Y.-L. Liao, K.-T. Wong, C.-I. Wu, *Adv. Mater.* **2006**, *18*, 1216-1220; b) H. Xu, L.-H. Wang, X.-H. Zhu, K. Yin, G.-Y. Zhong, X.-Y. Hou, W. Huang, *J. Phys. Chem. B* **2006**, *110*, 3023-3029; c) C.-F. Chang, Y.-M. Cheng, Y. Chi, Y.-C. Chiu, C.-C. Lin, G.-H. Lee, P.-T. Chou, C.-C. Chen, C.-H. Chang, C.-C. Wu, *Angew. Chem. Int. Ed.* **2008**, *47*, 4542-4545; d) Y.-C. Chiu, J.-Y. Hung, Y. Chi, C.-C. Chen, C.-H. Chang, C.-C. Wu, Y.-M. Cheng, Y.-C. Yu, G.-H. Lee, P.-T. Chou, *Adv. Mater.* **2009**, *21*, 2221-2225; e) C.-H. Chang, C.-C. Chen, C.-C. Wu, C.-H. Yang, Y. Chi, *Org. Electron.* **2009**, *10*, 1364-1371; f) C.-H. Lin, Y.-Y. Chang, J.-Y. Hung, C.-Y. Lin, Y. Chi, M.-W. Chung, C.-L. Lin, P.-T. Chou, G.-H. Lee, C.-H. Chang, W.-C. Lin, *Angew. Chem. Int. Ed.* **2011**, *50*, 3182-3186; g) Q. Zhang, T. Komino, S. Huang, S. Matsunami, K. Goushi, C. Adachi, *Adv. Funct. Mater.* **2012**, *22*, 2327-2336.

[20] a) S.-J. Su, T. Chiba, T. Takeda, J. Kido, *Adv. Mater.* **2008**, *20*, 2125-2130; b) S.-J. Su, Y. Takahashi, T. Chiba, T. Takeda, J. Kido, *Adv. Funct. Mater.* **2009**, *19*, 1260-1267.

[21] C.-H. Chang, C.-C. Chen, C.-C. Wu, S.-Y. Chang, J.-Y. Hung, Y. Chi, *Org. Electron.* **2010**, *11*, 266-272.

[22] B. Tong, H. Y. Ku, I. J. Chen, Y. Chi, H.-C. Kao, C.-C. Yeh, C.-H. Chang, S.-H. Liu, G.-H. Lee, P.-T. Chou, *J. Mater. Chem. C* **2015**, *3*, 3460-3471.

[23] a) M. G. Helander, Z. B. Wang, J. Qiu, M. T. Greiner, D. P. Puzzo, Z. W. Liu, Z. H. Lu, *Science* **2011**, *332*, 944-947; b) Y.-S. Park, S. Lee, K.-H. Kim, S.-Y. Kim, J.-H. Lee, J.-J. Kim, *Adv. Funct. Mater.* **2013**, *23*, 4914-4920.

[24] a) C.-H. Chang, K.-C. Tien, C.-C. Chen, M.-S. Lin, H.-C. Cheng, S.-H. Liu, C.-C. Wu, J.-Y. Hung, Y.-C. Chiu, Y. Chi, *Org. Electron.* **2010**, *11*, 412-418; b) K.-Y. Liao, C.-W. Hsu, Y. Chi, M.-K. Hsu, S.-W. Wu, C.-H. Chang, S.-H. Liu, G.-H. Lee, P.-T. Chou, Y. Hu, N. Robertson, *Inorg. Chem.* **2015**, *54*, 4029-4038.

[25] H.-H. Yeh, S.-T. Ho, Y. Chi, J. N. Clifford, E. Palomares, S.-H. Liu, P.-T. Chou, *J. Mater. Chem. A* **2013**, *1*, 7681-7689.

[26] J.-L. Liao, Y. Chi, J.-Y. Wang, Z.-N. Chen, Z.-H. Tsai, W.-Y. Hung, M.-R. Tseng, G.-H. Lee, *Inorg. Chem.* **2016**, *55*, 6394-6404.

[27] M. J. Frisch, G. W. Trucks, H. B. Schlegel, G. E. Scuseria, M. A. Robb, J. R. Cheeseman, G. Scalmani, V. Barone, B. Mennucci, G. A. Petersson, H. Nakatsuji, M. Caricato, X. Li, H. P. Hratchian, A. F. Izmaylov, J. Bloino, G. Zheng, J. L. Sonnenberg, M. Hada, M. Ehara, K. Toyota, R. Fukuda, J. Hasegawa, M. Ishida, T. Nakajima, Y. Honda, O. Kitao, H. Nakai, T. Vreven, J. A. Montgomery,

J. E. Peralta, F. Ogliaro, M. Bearpark, J. J. Heyd, E. Brothers, K. N. Kudin, V. N. Staroverov, R. Kobayashi, J. Normand, K. Raghavachari, A. Rendell, J. C. Burant, S. S. Iyengar, J. Tomasi, M. Cossi, N. Rega, J. M. Millam, M. Klene, J. E. Knox, J. B. Cross, V. Bakken, C. Adamo, J. Jaramillo, R. Gomperts, R. E. Stratmann, O. Yazyev, A. J. Austin, R. Cammi, C. Pomelli, J. W. Ochterski, R. L. Martin, K. Morokuma, V. G. Zakrzewski, G. A. Voth, P. Salvador, J. J. Dannenberg, S. Dapprich, A. D. Daniels, Ö. Farkas, J. B. Foresman, J. V. Ortiz, J. Cioslowski, D. J. Fox, *Gaussian 09, Revision D.01; Gaussian Inc.* **2013**, Wallingford, CT.

[28] a) A. D. Becke, *J. Chem. Phys.* **1993**, *98*, 5648-5652; b) C. Lee, W. Yang, R. G. Parr, *Phys. Rev. B* **1988**, *37*, 785-789.

[29] P. J. Hay, W. R. Wadt, *J. Chem. Phys.* **1985**, *82*, 299-310.

[30] a) G. A. Petersson, A. Bennett, T. G. Tensfeldt, M. A. Al-Laham, W. A. Shirley, J. Mantzaris, *J. Chem. Phys.* **1988**, *89*, 2193-2218; b) G. A. Petersson, M. A. Al-Laham, *J. Chem. Phys.* **1991**, *94*, 6081-6090.

[31] J. Tomasi, B. Mennucci, E. Cancès, *J. Mol. Struct. (Theochem)* **1999**, *464*, 211-226.

[32] S. Grimme, J. Antony, S. Ehrlich, H. Krieg, *J. Chem. Phys.* **2010**, *132*, 154104.

[33] N. M. O'Boyle, A. L. Tenderholt, K. M. Langner, *J. Comput. Chem.* **2008**, *29*, 839-845.

[34] A.-R. Allouche, *J. Comput. Chem.* **2011**, *32*, 174-182.

[35] J. Lin, N.-Y. Chau, J.-L. Liao, W.-Y. Wong, C.-Y. Lu, Z.-T. Sie, C.-H. Chang, M. A. Fox, P. J. Low, G.-H. Lee, Y. Chi, *Organometallics* **2016**, *35*, 1813-1824.

[36] A. P. Scott, L. Radom, *J. Phys. Chem.* **1996**, *100*, 16502-16513.

[37] A. E. Aliev, D. Courtier-Murias, S. Zhou, *J. Mol. Struct. (Theochem)* **2009**, *893*, 1-5.